Immunity

Article

Maternal gut bacteria drive intestinal inflammation in offspring with neurodevelopmental disorders by altering the chromatin landscape of CD4^{+} T cells

Graphical abstract

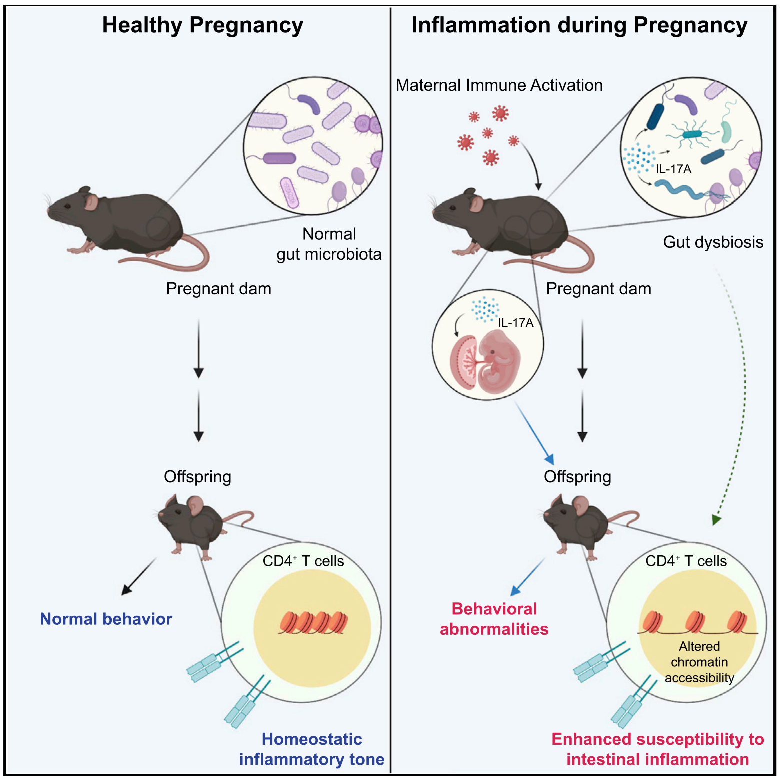

Highlights

- Mice prenatally exposed to maternal immune activation display immune-primed phenotypes
- Maternal immune activation induces changes in the gut microbiota of pregnant mice
- Altered microbiota promote immune priming by affecting T cells' chromatin accessibility
- Maternal IL-17A shapes the immune-primed phenotypes through changes in microbiota

Authors

Eunha Kim, Donggi Paik, Ricardo N. Ramirez, ..., Ho-Keun Kwon, Gloria B. Choi, Jun R. Huh

Correspondence

gbchoi@mit.edu (G.B.C.),
jun_huh@hms.harvard.edu (J.R.H.)

In brief

Children with autism spectrum disorders often display dysregulated immune responses. Using a preclinical mouse model manifesting neurodevelopmental pathologies following exposure to maternal immune activation, Kim et al. revealed that changes in the gut microbiota of pregnant mice affect chromatin accessibility of naive CD4^{+} T cells in their offspring, leading to immune-primed phenotypes.

Kim et al., 2022, Immunity *55*, 145–158
January 11, 2022
https://doi.org/10.1016/j.immuni.2021.11.005

Immunity

CellPress

Article

Maternal gut bacteria drive intestinal inflammation in offspring with neurodevelopmental disorders by altering the chromatin landscape of CD4$^+$ T cells

Eunha Kim,[1,6] Donggi Paik,[1,6] Ricardo N. Ramirez,[1] Delaney G. Biggs,[1] Youngjun Park,[1,4] Ho-Keun Kwon,[1,5] Gloria B. Choi,[2,*] and Jun R. Huh[1,3,7,*]

[1]Department of Immunology, Blavatnik Institute, Harvard Medical School, Boston, MA 02115, USA

[2]The Picower Institute for Learning and Memory, Department of Brain and Cognitive Sciences, Massachusetts Institute of Technology, Cambridge, MA 02139, USA

[3]Evergrande Center for Immunologic Diseases, Harvard Medical School and Brigham and Women's Hospital, Boston, MA 02115, USA

[4]Present address: Department of Pharmacy, College of Pharmacy, Jeju National University, Jeju Special Self-Governing Province 63243, Republic of Korea

[5]Present address: Department of Microbiology and Immunology, Institute for Immunology and Immunological Diseases and Brain Korea 21 PLUS Project for Medical Sciences, Yonsei University College of Medicine, Seoul 03722, Republic of Korea

[6]These authors contributed equally

[7]Lead contact

*Correspondence: gbchoi@mit.edu (G.B.C.), jun_huh@hms.harvard.edu (J.R.H.)

https://doi.org/10.1016/j.immuni.2021.11.005

SUMMARY

Children with autism spectrum disorders often display dysregulated immune responses and related gastrointestinal symptoms. However, the underlying mechanisms leading to the development of both phenotypes have not been elucidated. Here, we show that mouse offspring exhibiting autism-like phenotypes due to prenatal exposure to maternal inflammation were more susceptible to developing intestinal inflammation following challenges later in life. In contrast to its prenatal role in neurodevelopmental phenotypes, interleukin-17A (IL-17A) generated immune-primed phenotypes in offspring through changes in the maternal gut microbiota that led to postnatal alterations in the chromatin landscape of naive CD4$^+$ T cells. The transfer of stool samples from pregnant mice with enhanced IL-17A responses into germ-free dams produced immune-primed phenotypes in offspring. Our study provides mechanistic insights into why children exposed to heightened inflammation in the womb might have an increased risk of developing inflammatory diseases in addition to neurodevelopmental disorders.

INTRODUCTION

Prenatal and early life experiences are critical determinants for human health (Wadhwa et al., 2009). Human epidemiological studies have suggested an association between early life exposure to adverse conditions, including a maternal high-fat diet, malnutrition, or infection during pregnancy, and the development of various inflammatory and metabolic diseases as well as neurodevelopmental disorders (Gluckman et al., 2008; Kellermayer, 2012; Lee et al., 2015; Moore et al., 2006). Notably, multiple studies have suggested that viral infection during pregnancy correlates with an increased frequency of autism spectrum disorder (ASD) in offspring (Atladóttir et al., 2010; Lee et al., 2015). Intriguingly, individuals with ASD are also known to display a broad range of non-neurological comorbidities, including immune and gastrointestinal (GI) dysfunction (Doshi-Velez et al., 2015; Kohane et al., 2012; Mead and Ashwood, 2015). Signs of inflammation include elevated production of inflammatory cytokines, lymphoid nodular hyperplasia, and intestinal pathologies, such as enterocolitis (Buie et al., 2010; Coury et al., 2012; Hsiao, 2014). However, the mechanisms by which inflammatory phenotypes manifest as comorbid symptoms of neurodevelopmental disorders are largely unknown.

To address this question, we investigated the long-term immunological consequences using an established rodent model in which maternal immune activation (MIA) is induced in pregnant mice by injecting them intraperitoneally with the viral mimetic polyinosinic:polycytidylic acid (poly[I:C]) at embryonic day 12.5 (E12.5). Offspring from MIA mothers exhibit behavioral phenotypes, such as sociability deficits and repetitive behaviors (Choi et al., 2016; Smith et al., 2007). Here, we demonstrated that MIA offspring also possessed epigenetically primed CD4$^+$ T cells, which readily differentiate into inflammatory T effector cells upon exposure to a lymphopenic condition or a bacterial infection and exhibited heightened susceptibility to developing colitis-like and other inflammatory phenotypes. Unlike behavioral phenotypes that are prenatally determined (Kim et al., 2017), cross-fostering experiments suggested that the immunological phenotypes of MIA offspring were postnatally determined. We further showed that the observed immune-primed phenotypes of MIA offspring were dictated by the changes in the maternal gut microbiota and depended on maternal IL-17A, the same cytokine that drives MIA-associated behavioral and neurological phenotypes in offspring (Choi et al., 2016). Lastly, we demonstrate that the induction of immune-primed phenotypes in MIA offspring could be dissociated from that of neurodevelopmental phenotypes. The development of immune-primed phenotypes in offspring was selectively prevented when pregnant MIA dams lacked a complex microbial community, while only those phenotypes were induced when germ-free (GF) dams were colonized with the gut microbiota from MIA-exposed, conventionally reared pregnant dams. These data collectively provide insight into the mechanism by which exposure to enhanced inflammation during pregnancy can lead to long-lasting neurodevelopmental as well as immune-primed phenotypes in a subset of individuals with ASD.

RESULTS

Prenatal exposure to maternal inflammation increases susceptibility to bacteria-induced gut inflammation

To examine if MIA contributes to enhanced susceptibility to inflammation, adult offspring born to PBS- and poly(I:C)-injected mothers (hereafter referred to as PBS- and MIA-offspring) were subjected to a *Citrobacter rodentium* infection, a bacterial-induced colitis model used to study mucosal immune responses (Silberger et al., 2017) (Figure 1A). PBS and MIA offspring, at steady state, displayed similar body weight, colon length, and percentages of $CD4^+$ T cells in the lamina propria of colons and small intestines (Figures S1A–S1E). To minimize the heterogeneity in the composition of gut commensal bacteria that could act unfavorably to *C. rodentium* infection (Osbelt et al., 2020), we orally pre-treated mice with metronidazole (Figure 1A) as previously reported (Wlodarska et al., 2011). Colon length and the proportion of lamina propria $CD4^+$ T cells remained comparable in PBS and MIA offspring after the metronidazole treatment (Figure S2A). Subsequent *C. rodentium* infection did not change the body weight of both MIA and PBS offspring (Figure S2B). Bacterial loads in the colon, assessed by colony-forming units (CFUs) and qPCR for *espB* essential for *C. rodentium*'s colonization and pathogenesis (Sagaidak et al., 2016), were also similar between MIA and PBS offspring. (Figures 1B and S2C). However, when assessed 10 days after the infection, MIA offspring exhibited exacerbated gut inflammatory phenotypes, such as colon shortening (Figure 1C) and hyperplastic crypts in the colon (Figure 1D), compared to PBS offspring. These gut phenotypes were accompanied by systemic induction of interferon-gamma (IFN-γ) and interleukin-17A (IL-17A) (Figure 1E). In keeping with these inflammatory phenotypes, *C. rodentium* infection significantly increased the proportion of colonic IL-17A-producing and IL-17A- and IFN-γ-producing T cells (Lee et al., 2012) in MIA offspring compared to PBS offspring (Figures 1F, 1G, and 1I). In contrast, the proportion of $FoxP3^+$ regulatory T cells (Tregs) was reduced in MIA offspring (Figures 1H and 1I). Enhanced inflammatory phenotypes in MIA offspring were no longer observed 14 days after *C. rodentium* infection when bacterial-induced inflammatory responses plateaued (Bouladoux et al., 2017) (Figures S2D–S2F). These data suggest that prenatal exposure to MIA leads to mild but significantly accelerated immune responses in offspring when challenged with bacterial infection later in life. Of note, the MIA-induced increases in the expression of inflammatory cytokines were present in both male and female offspring (Figure S2G), unlike the MIA-associated neurodevelopmental phenotypes, which are preferentially induced in males (Kalish et al., 2021).

We next tested if MIA offspring's heightened inflammatory responses could be generalized to other immune challenges. PBS and MIA offspring were subjected to dextran sulfate sodium (DSS)-containing water or injected with anti-CD3 antibodies. DSS treatment stimulates innate immune responses and induces colitis-like phenotypes in colons (Dieleman et al., 1994), while anti-CD3 injection leads to T cell activation followed by a robust Th17 cell expansion in the duodenum (Esplugues et al., 2011). Unlike *C. rodentium* infection, the severity of DSS-induced pathological phenotypes in the colons was similar between MIA and PBS offspring (Figures S3A–S3C). In contrast, anti-CD3 treatments led to a higher proportion of Th17 cells in the duodenum of MIA offspring, although the extent of weight loss was similar to that of PBS offspring (Figures S3D and S3E). MIA offspring were also found with more severe disease phenotypes following induction of experimental autoimmune encephalomyelitis (EAE), an autoimmune disease model caused by pathogenic Th17 cells (Figure S3F). Taken together, these results indicate that MIA offspring exhibit immune-primed phenotypes, including enhanced production of IL-17A following exposure to certain, but not all, immune stimuli.

The immune-primed phenotypes of MIA offspring are postnatally, not prenatally, shaped by mothers

To determine whether MIA generates the immune-primed phenotypes in MIA offspring by acting pre- or postnatally, we next performed cross-fostering experiments in which pups born to PBS- and poly(I:C)-treated mothers were switched at birth (Figure 2A). As we have previously shown (Kim et al., 2017), MIA-induced behavioral abnormalities, such as reduced social preference (measured by the three-chamber assay) and enhanced repetitive behavior (measured by the marble-burying test), were not influenced by cross-fostering; offspring born to MIA dams but cross-fostered to PBS dams (MIAo-PBSd) still presented with sociability deficits and enhanced marble-burying behaviors, while offspring born to PBS dams cross-fostered to MIA dams (PBSo-MIAd) did not display these behavioral abnormalities (Figures 2B–2D). In contrast, inflammatory phenotypes induced by *C. rodentium* infection were dictated by the treatment conditions of foster mothers; both PBS and MIA offspring reared by MIA dams (PBSo-MIAd and MIAo-MIAd) exhibited shortened length and exacerbated histopathology of the colons when compared to PBS and MIA offspring reared by PBS dams (PBSo-PBSd and MIAo-PBSd) (Figures 2E and 2F). Furthermore, the percentage of colonic IL-17A and IFN-γ-producing Th17 cells was significantly higher, while the percentage of $FoxP3^+$ Tregs was reduced in offspring reared by MIA dams (Figure 2G). Therefore, immune-primed phenotypes in MIA offspring are likely acquired postnatally, and this is in contrast to their

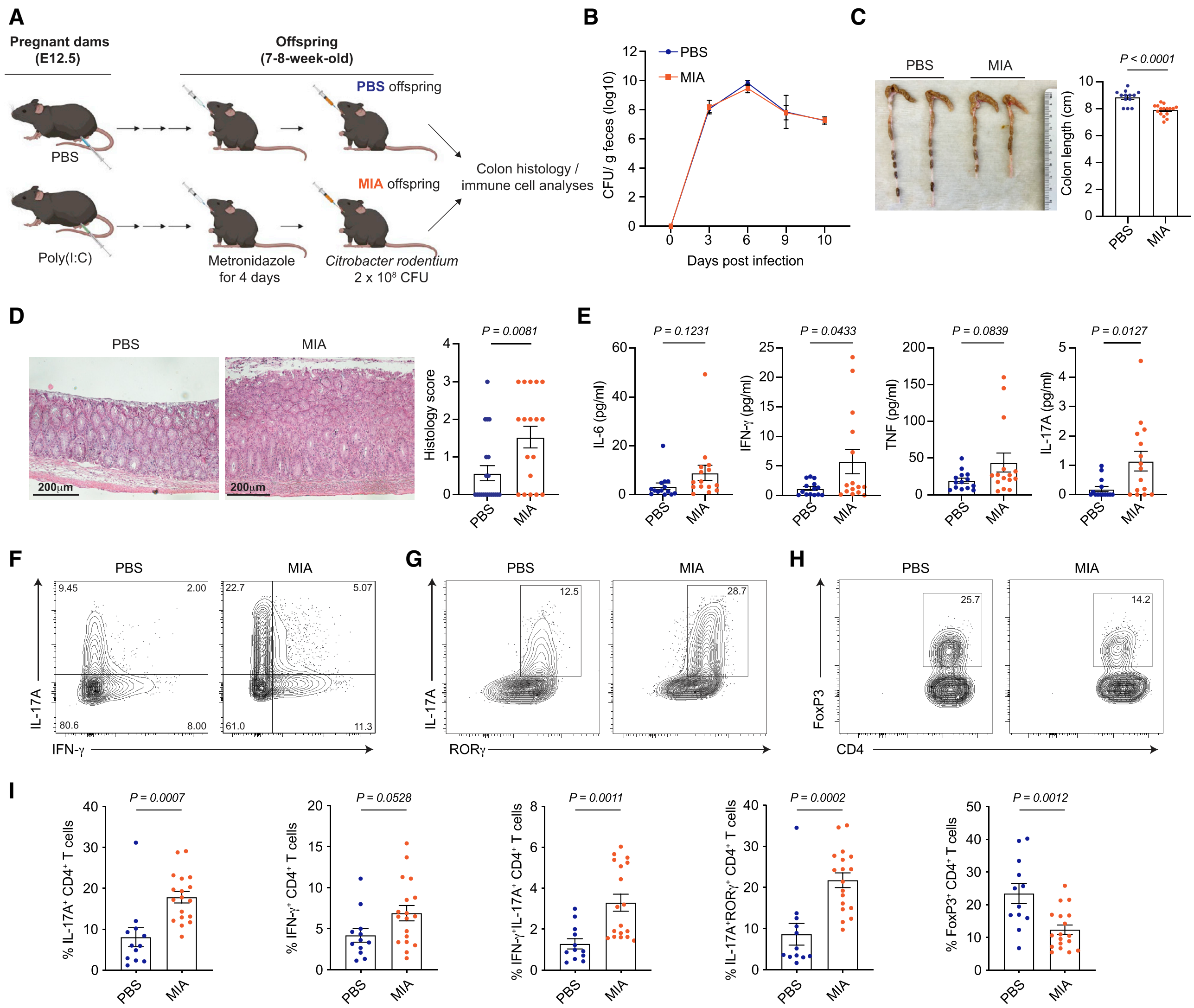

Figure 1. MIA offspring show increased susceptibility to bacteria-induced gut inflammation

(A) Seven- to eight-week-old offspring (PBS and MIA offspring) born to PBS- or poly(I:C)-injected dams at E12.5 were pre-treated with metronidazole for four days and then infected with 2×10^8 colony forming units (CFUs) of *C. rodentium.* All analyses were done ten days post-infection with *C. rodentium*.

(B) CFUs of *C. rodentium* were counted from the feces of infected PBS and MIA offspring over the course of infection (day 0: n = 5, 5; day 3: n = 8, 6; day 6: n = 10, 8; day 9: n = 8, 6; day 10: n = 10, 14).

(C–E) Colon length (n = 13, 16) (C), H&E staining of the colons, and the associated histology scores (n = 21, 18) (D), and plasma cytokine concentrations by cytometric bead array analyses (n = 14, 15) (E) of PBS and MIA offspring.

(F–I) The composition of colonic lamina propria T cells was analyzed by flow cytometry. Representative flow plots of IL-17A- and IFN-γ-producing $CD4^+$ T cells (F), $ROR\gamma^+$ IL-17A-producing $CD4^+$ T cells (G), $FoxP3^+$ regulatory T cells (H), and their quantifications (n = 12, 18) (I). All flow plots were gated on live, $CD45^+$, $TCR\beta^+$, $CD4^+$, $CD8^-$, and $CD19^-$ cells.

Data are shown as the mean ± SEM. p values were calculated by two-way ANOVA followed by Sidak's multiple comparison test (B) and Student's t tests (C–I). All data are combined from at least two independent experiments.

See Table S1 for detailed statistics. See also Figures S1–S3.

behavioral abnormalities, which are determined prenatally (Figures 2B–2D; Kim et al., 2017).

Maternal gut microbiota are sufficient to produce long-lasting, immune-primed phenotypes in offspring

We next sought to identify maternal factors that can postnatally drive the immune-primed phenotypes in MIA offspring. Maternal microbiota have been appreciated as a critical contributor in shaping the offspring's immune system (De Agüero et al., 2016; Gensollen et al., 2016). We therefore first asked if MIA induces changes in the composition of gut bacteria in pregnant dams. Stool samples collected from pregnant mice following PBS or poly(I:C) injection were subjected to 16S ribosomal RNA (rRNA) sequencing analyses. We found that alpha diversity (Shannon diversity index, a measure of species richness and evenness) was diminished in MIA dams compared to PBS

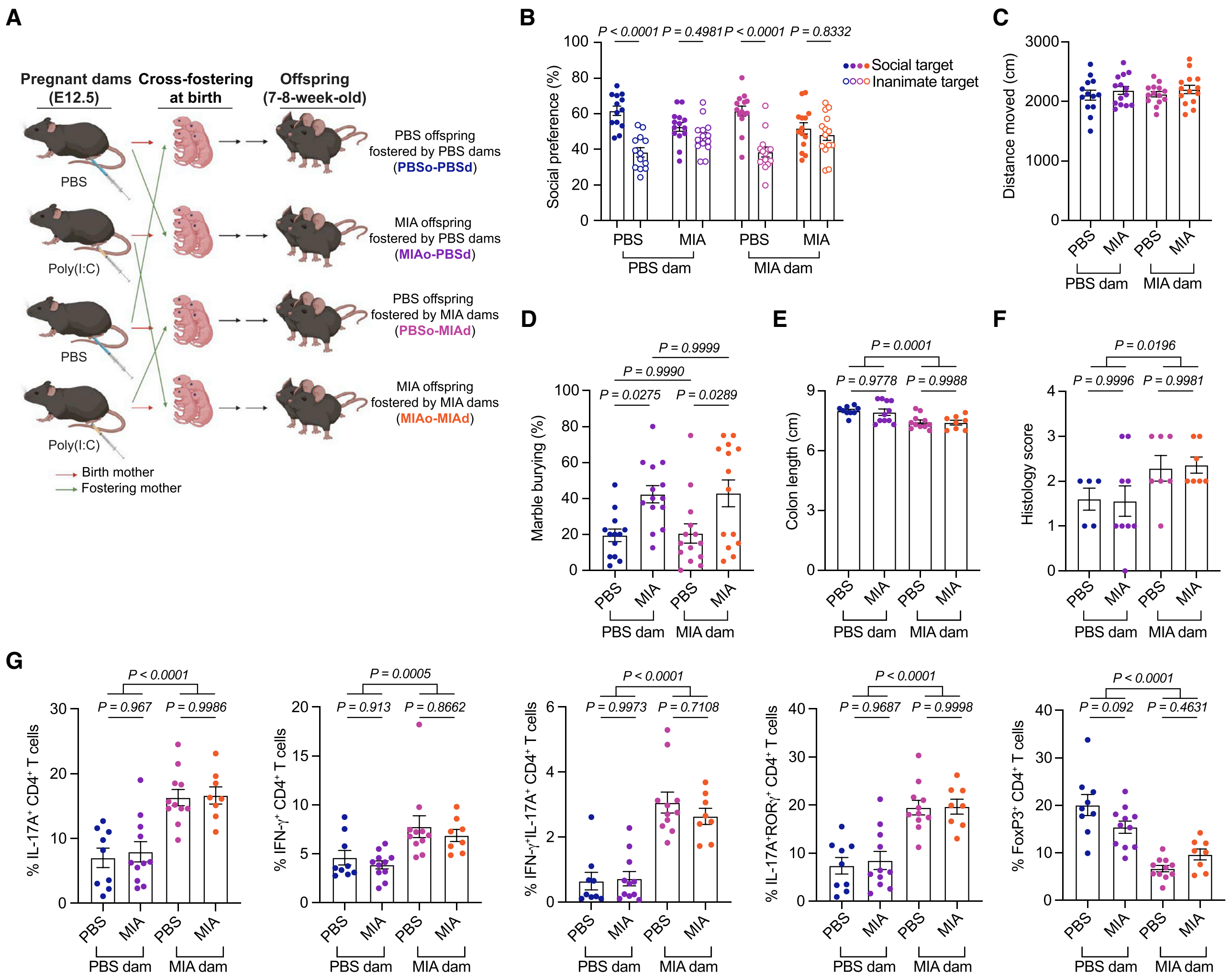

Figure 2. The increased immune susceptibility of MIA offspring is postnatally determined

(A) PBS and MIA offspring were cross-fostered upon birth (postnatal day 0 [P0]). Seven- to eight-week-old offspring were used for behavioral tests, followed by *C. rodentium* infection experiments, as described in Figure 1A.

(B and C) Percentage of interaction (B) and total distance moved (C) in the three-chamber sociability test of PBSo-PBSd, MIAo-PBSd, PBSo-MIAd, and MIAo-MIAd offspring (n = 13, 14, 14, 14).

(D) Marble-burying index of PBSo-PBSd, MIAo-PBSd, PBSo-MIAd, and MIAo-MIAd offspring (n = 13, 14, 14, 14).

(E and F) Colon length (n = 9, 11, 11, 8) (E) and histology scores (n = 5, 9, 7, 7) (F).

(G) The composition of colonic lamina propria T cells was analyzed by flow cytometry. Quantifications of IL-17A-, IFN-γ-, and IL-17A- and IFN-γ-producing $CD4^+$ T cells, $ROR\gamma^+$ IL-17A-producing $CD4^+$ T cells, and $FoxP3^+$ regulatory T cells of PBSo-PBSd, MIAo-PBSd, PBSo-MIAd, and MIAo-MIAd offspring (n = 9, 11, 11, 8). All flow data were gated on live, $CD45^+$, $TCR\beta^+$, $CD4^+$, $CD8^-$, and $CD19^-$ cells.

Data are shown as the mean ± SEM. p values were calculated by two-way ANOVA followed by Sidak's multiple comparisons test within groups (B) and Tukey's multiple comparison test (C–G). All data are combined from at least two independent experiments.

See Table S1 for detailed statistics.

dams (Figure S4A). We also observed that beta diversity (Bray-Curtis dissimilarity matrix, a statistic used to quantify the compositional dissimilarity) was substantially different between MIA and PBS dams (Figure S4B).

To investigate the contributing roles of MIA-associated changes in the maternal gut microbiota in producing the immune-primed phenotypes of MIA offspring, stool samples collected from PBS or MIA dams at E14.5 were transferred to GF B6 female mice (PBS-ST [stool transferred] and MIA-ST dams, respectively). The microbial composition of MIA-ST dams displayed both a reduced alpha diversity (Figure S4C) and a distinct beta diversity (Figure S4D) compared to those of PBS-ST dams, mirroring the differences observed in the gut microbial communities of PBS versus MIA dams (Figures S4A and S4B). PBS-ST and MIA-ST female mice were then crossed with GF B6 male mice to produce offspring exposed to PBS- or MIA-associated maternal microbiota from birth (PBS-ST or MIA-ST offspring) (Figure 3A). Both PBS-ST and MIA-ST offspring did not show MIA-associated behavioral abnormalities, such as reduced sociability and enhanced repetitive behaviors (Figures

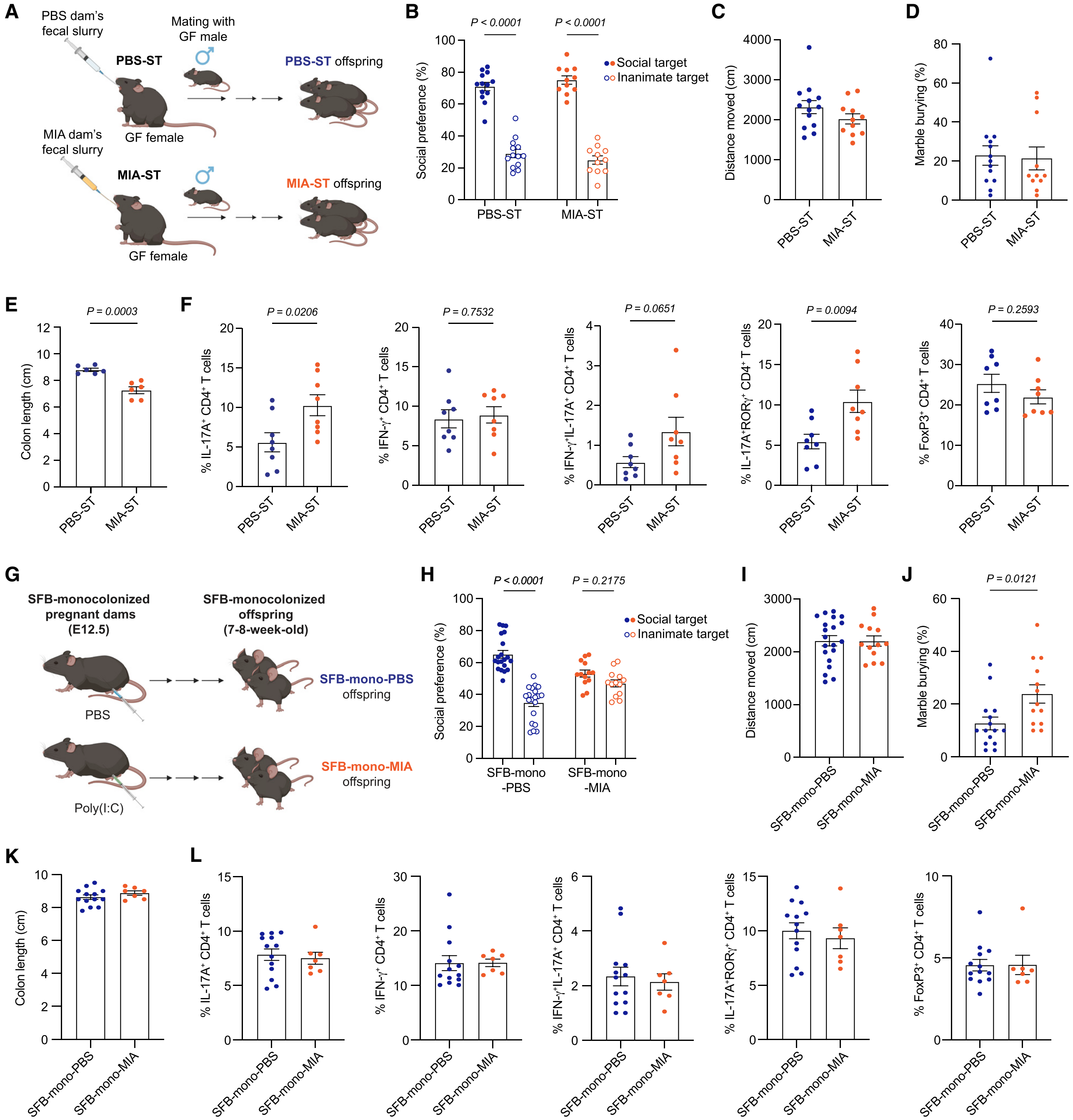

Figure 3. Transfer of MIA-associated microbiota induces primed immune phenotypes in offspring

(A) Female B6 GF mice were colonized with fecal bacteria of stool samples collected at E14.5 from either PBS or MIA dams (PBS-ST [stool-transferred] and MIA-ST, respectively) and a week later mated to male B6 GF mice. Offspring (PBS-ST offspring and MIA-ST offspring, respectively) from the mating were subjected to behavioral analyses followed by *C. rodentium* infection at seven to eight weeks of age.

(B and C) Percentage of interaction (B) and total distance moved (C) in the three-chamber sociability test of PBS-ST and MIA-ST offspring (n = 13, 11).

(D) Marble-burying index of PBS-ST and MIA-ST offspring (n = 13, 11).

(E) Colon length was measured ten days post-infection (n = 6 per group).

(F) The composition of colonic lamina propria T cells was analyzed by flow cytometry. Quantifications of IL-17A-, IFN-γ-, and both IL-17A- and IFN-γ-producing $CD4^+$ T cells, $ROR\gamma^+$ IL-17A-producing $CD4^+$ T cells, and $FoxP3^+$ regulatory T cells (n = 8 per group).

(G) SFB-mono-colonized B6 females were injected with PBS or poly(I:C) at E12.5. Offspring (SFB-mono-PBS and SFB-mono-MIA offspring, respectively) were subjected to behavioral analyses and followed by *C. rodentium* infection (1×10^6 CFUs) at seven to eight weeks of age.

(H and I) Percentage of interaction (H) and total distance moved (I) in the three-chamber sociability test of SFB-mono-PBS and SFB-mono-MIA offspring (n = 20, 13).

(legend continued on next page)

3B–3D). However, following *C. rodentium* infection, MIA-ST offspring exhibited heightened inflammatory phenotypes compared to PBS-ST, such as the shortened colon length (Figure 3E) and the increased proportion of IL-17A-producing T cells (Figure 3F). The percentages of FoxP3$^+$ Tregs in the colon remained comparable between the two groups (Figure 3F). Of note, we did not observe differences in the proportion of Th17 cells between MIA-ST and PBS-ST offspring at steady state. (Figures S4E and S4F). We next tested if bacterial colonization after weaning could similarly produce immune-primed phenotypes. GF mice, colonized with the stools of pregnant PBS and MIA dams upon weaning (PBS-ST-wean and MIA-ST-wean), did not display immune-primed phenotypes following *C. rodentium* infection (Figure S4G). These data suggest the existence of a developmental time frame in which MIA-associated maternal microbiota can exert changes in the immune phenotypes of their offspring.

To further examine the crucial role played by the maternal microbiota in establishing the offspring's immune status, we next injected PBS or poly(I:C) into B6 dams mono-colonized with segmented filamentous bacteria (SFB-mono-PBS and SFB-mono-MIA mice, respectively) (Figure 3G). SFB is a murine commensal known to promote Th17 cell differentiation in the small intestines (Ivanov et al., 2009), and its presence in pregnant dams kept at a specific pathogen-free condition has previously been shown to play a crucial role in the development of behavioral abnormalities in MIA offspring (Kim et al., 2017; Lammert et al., 2018). Consistent with these earlier findings, adult offspring born to the SFB-mono-MIA dams displayed both sociability deficits and enhanced marble-burying phenotypes (Figures 3H–3J). Unlike those born to conventionally reared dams (Figures 1C and 1F–1I), however, SFB-mono-PBS and SFB-mono-MIA offspring did not differ in the colon length or the percentages of IL-17A and IFN-γ-producing T cells and FoxP3$^+$ Tregs (Figures 3K and 3L). Therefore, SFB mono-colonization of dams was able to support the generation of neurodevelopmental, but not immunological, phenotypes in offspring. These data collectively support the idea that altered gut microbial community, rather than a single bacterial species capable of supporting a specific T cell response, in pregnant mice exposed to inflammation is both sufficient and necessary for the emergence of long-lasting, immune-primed phenotypes in MIA offspring.

MIA CD4$^+$ T cells are preferentially differentiated and activated into inflammatory effector T cells

We next probed for cell-intrinsic capacities of CD4$^+$ T cells from MIA offspring in inducing immune-primed phenotypes. We isolated CD45RB^{high} naive CD4$^+$ T cells (CD4$^+$, TCRβ^+, CD45RB^{high}, CD44^{low}, CD62L^{high}, CD25^{low}) from the spleens and lymph nodes (LNs) of MIA or PBS offspring (MIA-CD4$^+$ and PBS-CD4$^+$ T cells, respectively) and adoptively transferred them into immunocompromised RAG1-deficient mice. These mice provide a lymphopenic condition for transferred naive CD4$^+$ T cells to proliferate in response to gut-associated bacterial antigens and cause inflammation in the intestines (Powrie et al., 1993). To uncover the immune-primed nature of MIA-CD4$^+$ T cells, we transferred a relatively small number of T cells to recipient mice (Figure 4A). In this experimental condition, RAG1-deficient mice that received naive MIA-CD4$^+$ T cells lost weight, while the control PBS-CD4$^+$ group steadily, albeit modestly, gained weight during the five weeks post transfer (Figure 4B). Six weeks after the transfer, mice with MIA-CD4$^+$ T cells had shorter colons (Figure 4C) and displayed lymphocytic colitis signatures (Figure 4D). Additionally, a higher percentage of MIA-CD4$^+$ T cells were found to differentiate into Th17 cells compared to the PBS-CD4$^+$ T cells in the mesenteric LNs (MLNs) of the recipient mice (Figure S5A). We next performed T cell transfer experiments with naive CD4$^+$ T cells, isolated from cross-fostered PBS and MIA offspring (PBSo-MIAd and MIAo-PBSd, respectively) (Figure 2A) or from PBS-ST and MIA-ST offspring of stool-transferred GF dams (Figure 3A). Consistent with the results obtained from the CD4$^+$ T cells of MIA offspring (Figure S5A), higher percentages of transferred CD4$^+$ T cells from PBSo-MIAd and MIA-ST offspring produced IL-17A in RAG1-deficient mice compared to those from MIAo-PBSd and PBS-ST offspring, respectively (Figures S5B and S5C). Thus, MIA-induced changes in the maternal microbial community primed CD4$^+$ T cells in offspring for the higher production of IL-17A when exposed to a lymphopenic condition.

To assess transcriptomic changes associated with the primed immune status of MIA offspring, CD4$^+$ T cells isolated from congenically marked PBS and MIA offspring were transferred at a 1-to-1 ratio into the same RAG1-deficient mice. Four weeks after the transfer, transferred T cells were sorted from the MLNs of the recipient mice for bulk RNA sequencing (RNA-seq) (Figure 4E). RNA-seq and Gene Ontology (GO) analyses revealed increased expression of genes involved in T cell activation as well as T cell receptor signaling in MIA-CD4$^+$ T cells, including *Zbtb7a* (zinc finger and BTB domain-containing 7a), *Ifngr2* (interferon-gamma receptor 2), *Fcgr3* (Fc fragment of immunoglobulin G [IgG] receptor IIIa), *Syk* (spleen-associated tyrosine kinase), *Pik3r6* (phosphoinositide-3-kinase regulatory subunit 6), and *Tbx21* (T-box transcription factor 21) (Figures 4F and 4G). Furthermore, the gene set enrichment analysis (GSEA) similarly indicated that MIA-CD4$^+$ T cells are transcriptionally more poised to support MAPK activity, IL6-JAK-STAT3 signaling, and Th17 cell differentiation (Figures 4H and 4I). These data, taken together, suggest that CD4$^+$ T cells of MIA offspring are primed to express genes involved in T cell activation and T cell receptor signaling pathways upon exposure to a lymphopenic condition.

(J) Marble-burying index of SFB-mono-PBS and SFB-mono-MIA offspring (n = 15, 13).

(K) Colon length was measured ten days post-infection (n = 13, 7).

(L) The composition of colonic lamina propria T cells was analyzed by flow cytometry. Quantifications of IL-17A-, IFN-γ-, and both IL-17A- and IFN-γ-producing CD4$^+$ T cells, RORγ^+ IL-17A-producing CD4$^+$ T cells, and FoxP3$^+$ regulatory T cells (n = 13, 7). All flow data were gated on live, CD45$^+$, TCRβ^+, CD4$^+$, CD8$^-$, and CD19$^-$ cells.

Data are shown as the mean ± SEM. p values were calculated by two-way ANOVA followed by Sidak's multiple comparisons test within group (B and H) and Student's t tests (C–F and I–L). All data are combined from at least two independent experiments.

See Table S1 for detailed statistics. See also Figure S4.

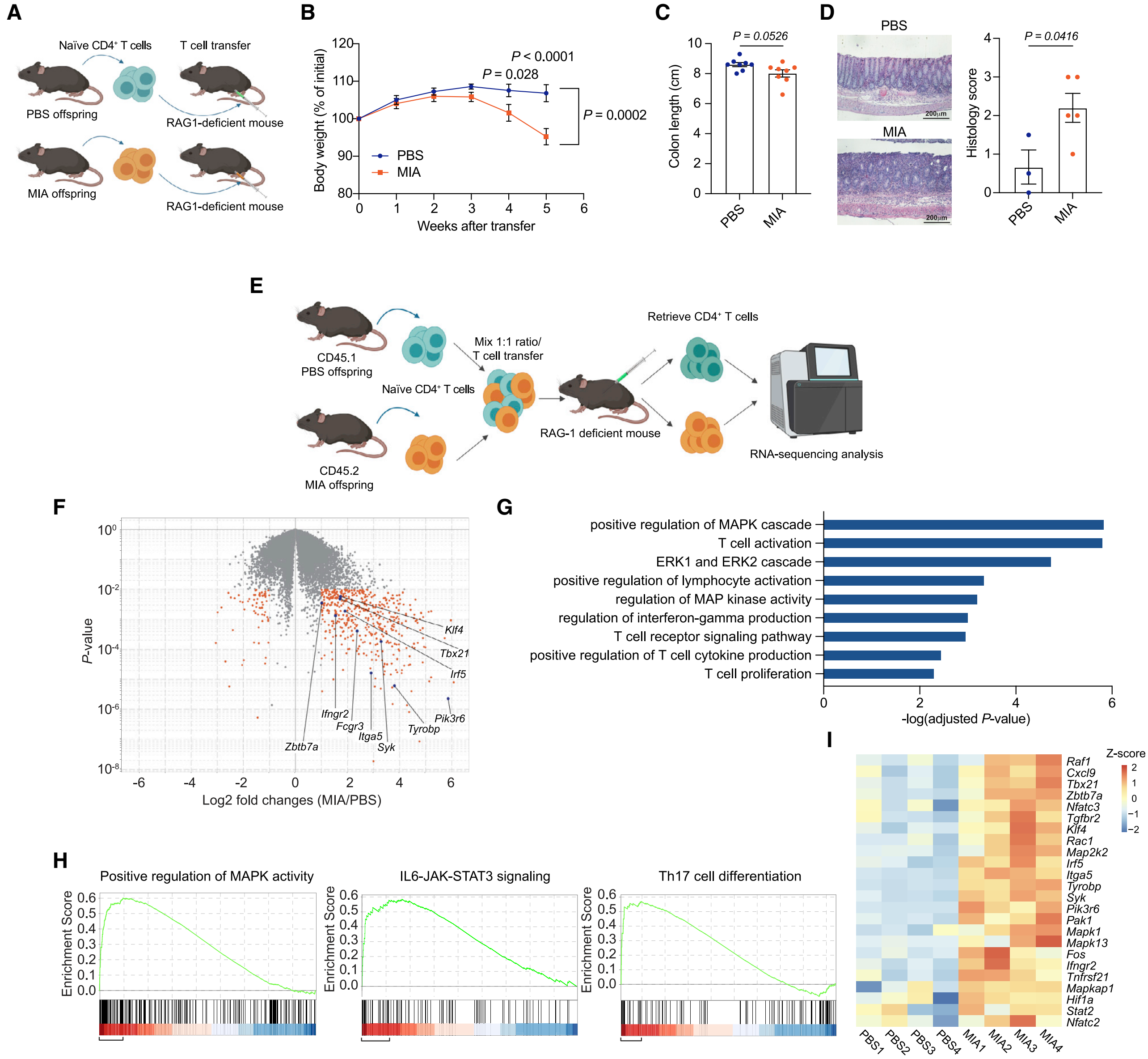

Figure 4. CD4+ T cells of MIA offspring display enhanced inflammatory phenotypes *in vivo*

(A) Naive $CD4^+$ T cells ($CD4^+$, $TCR\beta^+$, $CD45RB^{high}$, $CD44^{low}$, $CD62L^{high}$, and $CD25^{low}$) were isolated from the spleens and the lymph nodes of PBS and MIA offspring at 4 weeks of age, and 5×10^5 cells were transferred to RAG1-deficient mice.

(B) Body weight changes were monitored for five weeks (n = 15 per group).

(C and D) Measurement of the colon length (n = 8 per group) (C) and histological analysis with H&E staining (n = 3, 5) (D) were performed six weeks after the transfer.

(E) Naive $CD4^+$ T cells were isolated from four-week-old CD45.1 PBS and CD45.2 MIA offspring. PBS and MIA naive $CD4^+$ T cells were mixed in a 1:1 ratio and transferred into RAG1-deficient mice. Four weeks after transfer, transferred cells were retrieved, sorted by congenic markers, and analyzed by RNA sequencing.

(F) Volcano plot displaying log2 fold change (FC) versus p value for each gene. Genes considered significant ($p < 0.01$ and log2FC > 1) are labeled in orange, and selected genes involved in T cell activation and MAPK activity are labeled in blue.

(G) Graph showing the key GO terms that were enriched in the differentially expressed genes between PBS versus MIA $CD4^+$ T cells.

(H) GSEA analysis demonstrating significant enrichment of gene sets associated with MAPK activity, IL6-JAK-STAT3 signaling, and Th17 cell differentiation.

(I) Expression heatmap presenting genes highly expressed in the selected GSEA pathways.

Data are shown as the mean ± SEM. p values were calculated by two-way ANOVA followed by Bonferroni multiple comparisons test (B) and Student's t test (C and D).

See Table S1 for detailed statistics. See also Figure S5.

MIA CD4^{+} T cells are preferentially programmed to become inflammatory effector T cells

We next asked if the transcriptionally primed status of the MIA offspring's CD4^{+} T cells are similarly reflected in their chromatin structures by performing an assay for transposase-accessible chromatin with high-throughput sequencing (ATAC-seq) (Figure 5A). Naive CD4^{+} T cells from PBS and MIA offspring showed distinct chromatin accessibility; 101 ATAC peaks were uniquely found in PBS-CD4^{+} T cells, while 1,532 peaks were distinctively present in MIA-CD4^{+} T cells (Figures 5B and 5C; fold changes > 1.5, false discovery rate [FDR] < 0.05). The open peaks uniquely found in MIA-CD4^{+} T cells were enriched for functional clusters associated with the regulation of adaptive immune responses, epigenetic regulation, and regulation of kinase activity (Figure 5D). For example, the open peaks were of genes involved in T effector cell differentiation and activation, such as *Il6ra* (IL-6 receptor subunit alpha) (Harbour et al., 2020) and *Zbtb7a* (Carpenter et al., 2012). ATAC-seq also identified genes involved in chromatin remodeling, such as *Brd4* (bromodomain protein 4) (Devaiah et al., 2016), *Smarcd2* (SWI/SNF-related matrix-associated actin-dependent regulator of chromatin subfamily D member 2) (Witzel et al., 2017), and *Map4k2* (mitogen-activated kinase kinase kinase kinase 2) (Chuang et al., 2016), which is a member of the MAP4 kinase family associated with the regulation of T cell activity (Figure 5E). Accordingly, mRNA expression of these genes was elevated, albeit modestly, in MIA-CD4^{+} T cells (Figure 5F).

We observed that altered chromatin accessibility was also present in naive CD4^{+} T cells of offspring born to MIA-stool transferred dams (MIA-ST offspring) (Figure 3A). ATAC-seq revealed 84 and 483 peaks uniquely found in PBS-ST's and MIA-ST's CD4^{+} T cells, respectively (Figures S6A and S6B). Consistent with the ATAC-seq profiles observed in naive CD4^{+} T cells of MIA offspring (Figure 5D), the ATAC-seq peaks that were differentially present in MIA-ST's CD4^{+} T cells were enriched for those genes involved in the regulation of kinase activity and T cell activation (Figure S6C). These data, taken together, suggest that exposure to MIA-associated changes in maternal gut microbiota leads to changes in the chromatin landscape of naive CD4^{+} T cells in offspring to allow for their primed immune responses.

Maternally induced IL-17A is critical for immune susceptibility in offspring

We next examined the contributing roles of maternal IL-17A in promoting immune-primed phenotypes in MIA offspring. Previously, we found that MIA resulted in an increase in the plasma concentrations of IL-17A in pregnant mothers, and this increase was causal to the emergence of behavioral and neurological abnormalities observed in offspring (Choi et al., 2016). To test if maternal IL-17A also plays a role in generating offspring's immune-primed phenotypes, we injected pregnant mothers with IgG isotype control or anti-IL-17A blocking antibodies 5 h prior to treating them with PBS or poly(I:C) at E12.5 (Figure 6A). Offspring born to these mothers were then infected with *C. rodentium* at seven to eight weeks of age. When tested ten days after the infection, MIA offspring from poly(I:C)-injected mothers pre-treated with IL-17A blocking antibodies (MIA anti-IL-17A), but not with IgG isotype control antibodies (MIA isotype), showed comparable colon length to that of PBS offspring (PBS isotype) (Figure 6B). The proportion of Th17 cells, IFN-γ-producing pathogenic Th17 cells as well as the population of Tregs in MIA offspring from mothers treated with anti-IL-17A antibodies, also remained comparable to those of PBS control mice (PBS-isotype) (Figure 6C), indicating that maternal IL-17A plays a crucial role in mediating the exacerbated gut as well as immunological phenotypes seen in MIA offspring upon *C. rodentium* infection.

Next, we asked if the maternal microbiota's role in enhancing susceptibility to *C. rodentium*-induced colitis in MIA offspring was dependent on maternal IL-17A. Stool samples collected from PBS isotype, MIA isotype, or MIA anti-IL-17A antibody-treated dams at E14.5 were introduced to GF B6 female mice. The females were then crossed with GF B6 male mice to produce offspring exposed to PBS isotype-, MIA isotype-, or MIA anti-IL-17A-associated maternal microbiota from birth (PBS isotype-ST, MIA isotype-ST, or MIA anti-IL-17A-ST offspring) (Figure 6D). Following *C. rodentium* infection, MIA anti-IL-17A-ST offspring, unlike in MIA isotype-ST offspring, exhibited neither the shortened colon length nor an enhanced IL-17A production (Figures 6E and 6F). These results indicate that the MIA-induced increase of maternal IL-17A contributes to the primed immunological phenotypes observed in MIA offspring by altering the pregnant dam's gut microbiota community.

DISCUSSION

Earlier studies have reported that mouse offspring prenatally exposed to maternal inflammation display GI dysfunctions (Hsiao et al., 2013; Li et al., 2021). In addition, MIA offspring's immune cells have been shown to produce higher inflammatory cytokines upon activation both *in vitro* and *in vivo* (Hsiao et al., 2012; Reed et al., 2020). However, the causal driver of this augmentation has remained elusive. Our study identified the underlying mechanism by which *in utero* inflammation promotes the development of immune-primed phenotypes in offspring, in addition to the previously reported autism-like behavioral abnormalities (Choi et al., 2016; Malkova et al., 2012; Smith et al., 2007).

Our data also showed that, although both the immune and behavioral phenotypes observed in MIA offspring depended on the same maternal cytokine IL-17A, the mechanisms by which IL-17A transduces its effects into each of these phenotypes are distinct. We showed that the immune-primed phenotype in offspring was mediated through the IL-17A-induced changes in maternal gut microbiota. We further showed that these changes in maternal microbiota were sufficient to postnatally produce inflammatory phenotypes, likely by causing changes in the chromatin accessibility of offspring's naive CD4^{+} T cells. On the other hand, the behavioral abnormalities of MIA offspring require the expression of the IL-17 receptor in the embryonic brain and its activation during the prenatal period, as we previously reported (Kalish et al., 2021; Kim et al., 2017). Indeed, we were able to uncouple the behavioral abnormalities from the immune-primed phenotypes of MIA offspring by inducing MIA in SFB-mono-colonized mice or by transferring gut microbiota from MIA-exposed mothers into GF mice. Our data suggest that blocking IL-17A activity in pregnant women, who are vulnerable to inflammatory conditions during pregnancy, may be used

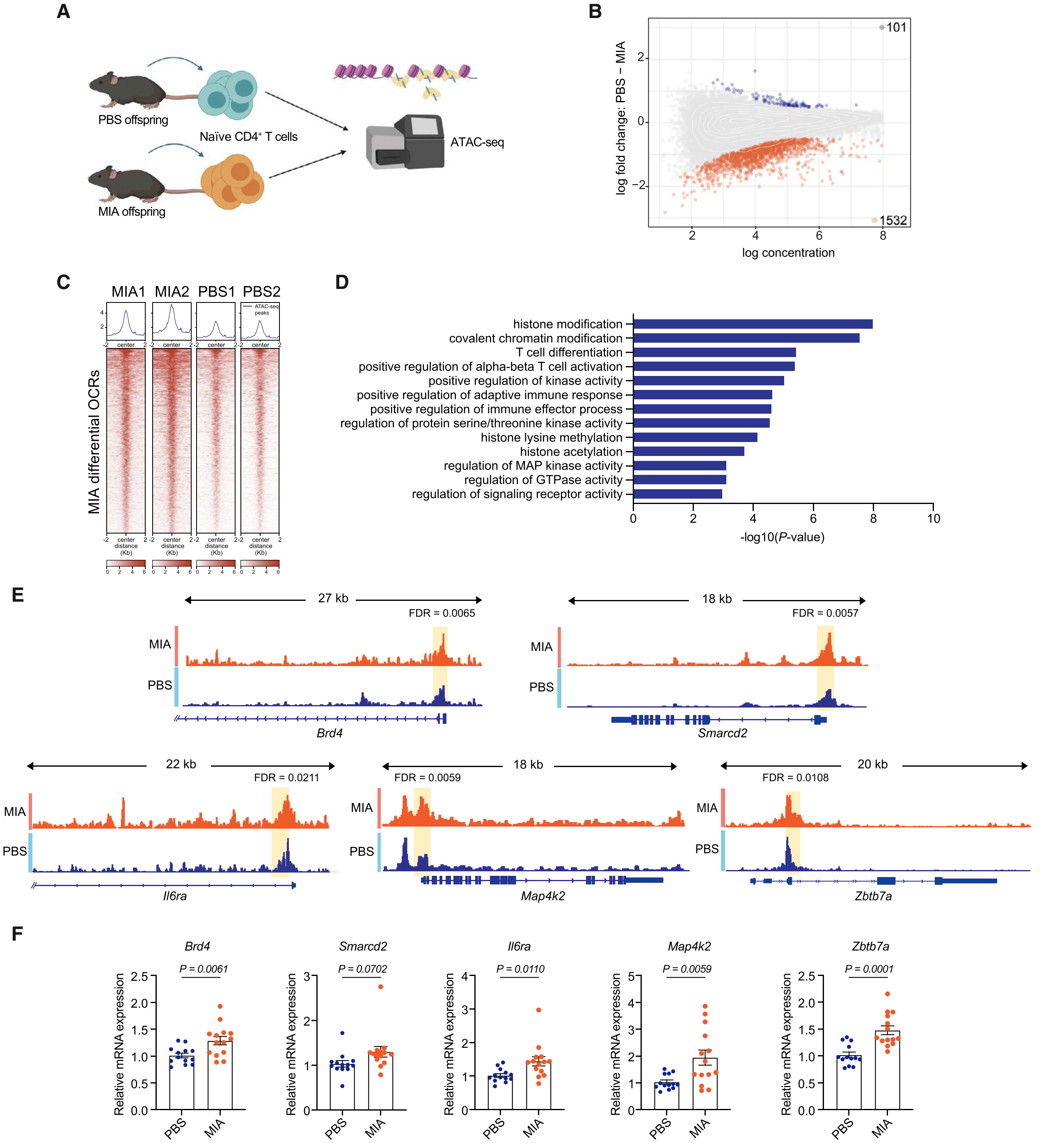

Figure 5. MIA naive CD4+ T cells display distinct chromatin accessibility

(A) Naive CD4+ T cells were isolated from four-week-old PBS and MIA offspring and subjected to ATAC-seq analyses.

(B) Scatterplot represents the differences in chromatin accessibility between PBS and MIA naive CD4+ T cells. Orange dots indicate peaks that are more accessible in MIA naive CD4+ T cells, and blue dots indicate those that are uniquely accessible in PBS naive CD4+ T cells (fold change > 1.5, FDR < 0.05).

(C) Heatmaps depicting differentially enriched ATAC-seq signals in MIA naive CD4+ T cells.

(D) GO terms that were enriched in the differential open chromatin regions (OCRs) of MIA naive CD4+ T cells compared to those of PBS offspring.

(E) Integrated genome viewer snapshots of representative genes involved in T cell differentiation, epigenetic regulation, and kinase activity. Genomic regions differentially open in MIA naive CD4+ T cells are highlighted in yellow boxes. Two offspring from different littermates per group were used for naive CD4+ T cell isolation.

(F) Quantitative PCR (qPCR) analyses for those genes shown in (E) (n = 13, 14).

Data are shown as the mean ± SEM. p values were calculated by Student's t test (F).

See Table S1 for detailed statistics. See also Figure S6.

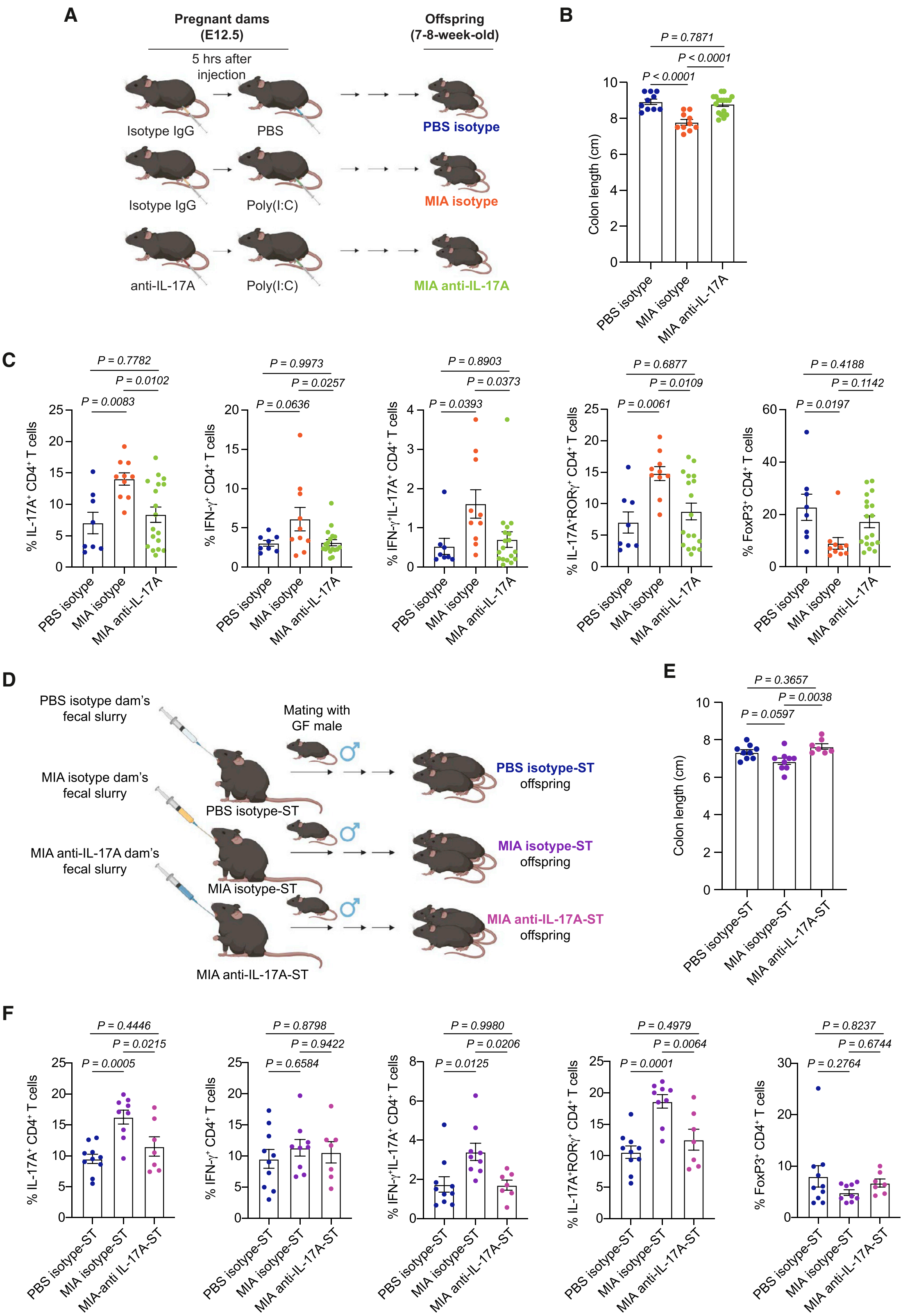

Figure 6. IL-17A-dependent changes in maternal gut microbiota promote inflammatory phenotypes in MIA offspring

(A) Poly(I:C)-injected dams were pre-treated either with isotype IgG or IL-17A blocking antibodies. Seven- to eight-week-old offspring (PBS isotype, MIA isotype, and MIA anti-IL-17A offspring) born to these dams were infected with 2×10^8 CFUs of *C. rodentium* as described in Figure 1A.

(legend continued on next page)

as therapeutic means to prevent the development of both neurodevelopmental and immunological disorders in offspring.

The coprophagic nature of rodents aids the vertical transmission of gut bacteria from pregnant mice to their offspring. Recent studies in humans report that the fecal microbiota of human pregnant mothers plays a critical role in shaping gut flora composition in newborn babies (Ferretti et al., 2018; Korpela et al., 2020; Wang et al., 2020). These data suggest that alterations in the gut microbiota of pregnant women who contract pathogens may also influence the long-term inflammatory phenotypes of their children through a similar mechanism that we described in the current study. How might the community of maternal microbiota affect the epigenetic landscape of offspring's T cells? While few earlier studies offer mechanistic insights, a recent work nicely illustrates that the early life colonization of intestinal bacteria could affect T cell development in the thymus (Zegarra-Ruiz et al., 2021). Maternally derived antibodies protect neonates against pathogens (Harris et al., 2006; Zinkernagel, 2001), shape an infant's microbial community (Gopalakrishna et al., 2019; Rios et al., 2016), and contribute to the development of RORγ^+ Tregs in offspring (Ramanan et al., 2020). During pregnancy, supplementation with probiotics, *Lactobacillus rhamnosus* or *Bifidobacterium lactis*, was shown to enhance immune-protective components in breast milk and modulate the fetal immune response (Prescott et al., 2008). The immune-associated alteration in maternal microbiota may result in changes in the composition of metabolites such as short-chain fatty acids (Koh et al., 2016) in breast milk, hence indirectly influencing immune responses in the affected offspring (Ganal-Vonarburg et al., 2020).

Overall, our study provided insight into how environmental stimuli, such as prenatal exposure to maternal inflammation, could dysregulate the offspring's immune system and render it more vulnerable to inflammatory challenges later in life. More specifically, it offered important insights into the occurrence of inflammatory dysfunctions that often accompany neurodevelopmental disorders. For example, our work suggested that a subset of individuals with ASD who manifest enhanced inflammatory phenotypes (Chaidez et al., 2014; Doshi-Velez et al., 2015; Kohane et al., 2012) might have been exposed to heightened inflammation in the maternal womb. Understanding the intricate interactions between the maternal gut and the offspring's neurodevelopment and immune system development will help us to better cope with the long-lasting effects of viral infections during pregnancy, including those of the current COVID-19 pandemic.

Limitations of the study

We performed our study using a mouse model in which administration of a double-stranded RNA induced inflammation during pregnancy. Therefore, it is unknown whether our findings can be generalized to other preclinical models for neurodevelopmental disorders that rely on different immune stimuli or genetic perturbations. Future studies are also needed to elucidate mechanisms by which changes in maternal gut microbiota affect the chromatin accessibility of offspring's CD4$^+$ T cells. Lastly, whether exposure to prenatal inflammation such as viral infection induces long-lasting immunological phenotypes in humans remains to be examined.

STAR★METHODS

Detailed methods are provided in the online version of this paper and include the following:

- KEY RESOURCES TABLE
- RESOURCE AVAILABILITY
  - ○ Lead contact
  - ○ Materials availability
  - ○ Data and code availability
- EXPERIMENTAL MODEL AND SUBJECT DETAILS
  - ○ Mice
- METHOD DETAILS
  - ○ Maternal immune activation
  - ○ Citrobacter rodentium infection
  - ○ Cytometric bead array
  - ○ Isolation of lamina propria lymphocytes
  - ○ Flow cytometry
  - ○ Tissue histology
  - ○ Dextran sodium sulfate-induced colitis
  - ○ Experimental autoimmune encephalomyelitis model
  - ○ Anti-CD3 induced inflammation
  - ○ Three-chamber social approach assay
  - ○ Marble-burying test
  - ○ Cross-fostering experiments
  - ○ Germ-free mouse colonization
  - ○ Isolation of fecal bacterial microbiota and 16S rRNA gene sequencing analysis
  - ○ Adoptive transfer of CD45RB^{high} CD4$^+$ T cells
  - ○ RNA extraction and quantitative real-time PCR
  - ○ RNA-seq experiments
  - ○ ATAC-seq experiments
- QUANTIFICATION AND STATISTICAL ANALYSIS

(B) Colon length was measured ten days following the infection (n = 10, 10, 17).
(C) Ten days after *C. rodentium* infection, the composition of colonic lamina propria T cells was analyzed by flow cytometry. Quantifications of IL-17A-, IFN-γ-, and both IL-17A- and IFN-γ-producing CD4$^+$ T cells, RORγ^+ IL-17A-producing CD4$^+$ T cells, and FoxP3$^+$ regulatory T cells (n = 8, 10, 18).
(D) Female B6 GF mice were colonized with fecal bacteria of PBS isotype, MIA isotype or MIA anti-IL-17A-treated E14.5 dams and a week later mated to male B6 GF mice. Offspring from the mating were infected with 2×10^8 CFUs of *C. rodentium* at seven to eight weeks of age.
(E) Colon length (n = 9, 9, 7) was measured ten days following the infection.
(F) Ten days after *C. rodentium* infection, the composition of colonic lamina propria T cells was analyzed by flow cytometry. Quantifications of IL-17A-, IFN-γ-, and both IL-17A- and IFN-γ-producing CD4$^+$ T cells, RORγ^+ IL-17A-producing CD4$^+$ T cells, and FoxP3$^+$ regulatory T cells (n = 10, 9, 7) are shown. All flow plots were gated on live, CD45$^+$, TCRβ^+, CD4$^+$, CD8$^-$, and CD19$^-$ cells.
Data are shown as the mean ± SEM. p values were calculated by one-way ANOVA following Tukey's multiple comparisons test (B, C, E, and F). All data are combined from at least two independent experiments.
See Table S1 for detailed statistics.

SUPPLEMENTAL INFORMATION

Supplemental information can be found online at https://doi.org/10.1016/j.immuni.2021.11.005.

ACKNOWLEDGMENTS

We thank all Huh laboratory members for scientific comments; N. Lee and J. Vasquez for technical assistance in GF work; M. Trombly for scientific editing of the manuscript; R. Bronson and the Rodent Histopathology Core at Harvard Medical School for performing H&E analysis and disease scoring; P.M. Llopis and the MicRoN Core at Harvard Medical School for their expertise and instrument availability for imaging; and the Biopolymer facility Next-Generation Sequencing Core at Harvard Medical School for their expertise and instrument availability with ATAC-seq and 16S rRNA sequencing. E.K. was supported by the basic science research program through the National Research Foundation of Korea (NRF) funded by the Ministry of Education (2018R1A6A3A03010693). G.B.C. and J.R.H. were supported by the Jeongho Kim Neurodevelopmental Research Fund, the Simons Foundation Autism Research Initiative, and National Institute of Mental Health grants (R01MH115037 and R01MH119459, respectively). J.R.H. was also supported by the N of One: Autism Research Foundation and the Burroughs Wellcome Fund. Earlier work included in this study was made possible by the support from the Kenneth Rainin Foundation to J.R.H. All schematic diagrams were created by Biorender.com.

AUTHOR CONTRIBUTIONS

G.B.C. and J.R.H. conceptualized the study. E.K., D.P., and J.R.H. designed experiments and analyzed data. E.K. and D.P. performed colitis experiments and analyzed immune cell function. E.K. performed behavioral experiments and analyzed RNA-seq data. E.K. and R.N.R. analyzed ATAC-seq data. D.G.B. maintained mice for the experiments. E.K., Y.P., and H.-K.K performed 16S bacterial sequencing. E.K., G.B.C., and J.R.H. wrote the manuscript.

DECLARATION OF INTERESTS

J.R.H. is a consultant for CJ Research Center, LLC, and is on the scientific advisory board for ChunLab.

Received: April 21, 2021
Revised: August 29, 2021
Accepted: November 10, 2021
Published: December 7, 2021

REFERENCES

De Agüero, M.G., Ganal-Vonarburg, S.C., Fuhrer, T., Rupp, S., Uchimura, Y., Li, H., Steinert, A., Heikenwalder, M., Hapfelmeier, S., Sauer, U., et al. (2016). The maternal microbiota drives early postnatal innate immune development. Science *351*, 1296–1302.

Atladóttir, H.O., Thorsen, P., Østergaard, L., Schendel, D.E., Lemcke, S., Abdallah, M., and Parner, E.T. (2010). Maternal infection requiring hospitalization during pregnancy and autism spectrum disorders. J. Autism Dev. Disord. *40*, 1423–1430.

Bolyen, E., Rideout, J.R., Dillon, M.R., Bokulich, N.A., Abnet, C.C., Al-Ghalith, G.A., Alexander, H., Alm, E.J., Arumugam, M., Asnicar, F., et al. (2019). Reproducible, interactive, scalable and extensible microbiome data science using QIIME 2. Nat. Biotechnol. *37*, 852–857.

Bouladoux, N., Harrison, O.J., and Belkaid, Y. (2017). The mouse model of infection with citrobacter rodentium. Curr. Protoc. Immunol. *2017*, 19.15.1–19.15.25.

Buenrostro, J.D., Giresi, P.G., Zaba, L.C., Chang, H.Y., and Greenleaf, W.J. (2013). Transposition of native chromatin for fast and sensitive epigenomic profiling of open chromatin, DNA-binding proteins and nucleosome position. Nat. Methods *10*, 1213–1218.

Buie, T., Campbell, D.B., Fuchs, G.J., 3rd, Furuta, G.T., Levy, J., Vandewater, J., Whitaker, A.H., Atkins, D., Bauman, M.L., Beaudet, A.L., et al. (2010). Evaluation, diagnosis, and treatment of gastrointestinal disorders in individuals with ASDs: a consensus report. Pediatrics *125* (*Suppl 1*), S1–S18.

Callahan, B.J., McMurdie, P.J., Rosen, M.J., Han, A.W., Johnson, A.J.A., and Holmes, S.P. (2016). DADA2: High-resolution sample inference from Illumina amplicon data. Nat. Methods *13*, 581–583.

Carpenter, A.C., Grainger, J.R., Xiong, Y., Kanno, Y., Chu, H.H., Wang, L., Naik, S., dos Santos, L., Wei, L., Jenkins, M.K., et al. (2012). The transcription factors Thpok and LRF are necessary and partly redundant for T helper cell differentiation. Immunity *37*, 622–633.

Chaidez, V., Hansen, R.L., and Hertz-Picciotto, I. (2014). Gastrointestinal problems in children with autism, developmental delays or typical development. J. Autism Dev. Disord. *44*, 1117–1127.

Choi, G.B., Yim, Y.S., Wong, H., Kim, S., Kim, H., Kim, S.V., Hoeffer, C.A., Littman, D.R., and Huh, J.R. (2016). The maternal interleukin-17a pathway in mice promotes autism-like phenotypes in offspring. Science *351*, 933–939.

Chuang, H.C., Wang, X., and Tan, T.H. (2016). MAP4K Family Kinases in Immunity and Inflammation (Elsevier Inc.).

Coury, D.L., Ashwood, P., Fasano, A., Fuchs, G., Geraghty, M., Kaul, A., Mawe, G., Patterson, P., and Jones, N.E. (2012). Gastrointestinal conditions in children with autism spectrum disorder: developing a research agenda. Pediatrics *130* (*Suppl 2*), S160–S168.

Devaiah, B.N., Case-Borden, C., Gegonne, A., Hsu, C.H., Chen, Q., Meerzaman, D., Dey, A., Ozato, K., and Singer, D.S. (2016). BRD4 is a histone acetyltransferase that evicts nucleosomes from chromatin. Nat. Struct. Mol. Biol. *23*, 540–548.

Dieleman, L.A., Ridwan, B.U., Tennyson, G.S., Beagley, K.W., Bucy, R.P., and Elson, C.O. (1994). Dextran sulfate sodium-induced colitis occurs in severe combined immunodeficient mice. Gastroenterology *107*, 1643–1652.

Doshi-Velez, F., Avillach, P., Palmer, N., Bousvaros, A., Ge, Y., Fox, K., Steinberg, G., Spettell, C., Juster, I., and Kohane, I. (2015). Prevalence of Inflammatory Bowel Disease Among Patients with Autism Spectrum Disorders. Inflamm. Bowel Dis. *21*, 2281–2288.

Esplugues, E., Huber, S., Gagliani, N., Hauser, A.E., Town, T., Wan, Y.Y., O'Connor, W., Jr., Rongvaux, A., Van Rooijen, N., Haberman, A.M., et al. (2011). Control of TH17 cells occurs in the small intestine. Nature *475*, 514–518.

Ferretti, P., Pasolli, E., Tett, A., Asnicar, F., Gorfer, V., Fedi, S., Armanini, F., Truong, D.T., Manara, S., Zolfo, M., et al. (2018). Mother-to-Infant Microbial Transmission from Different Body Sites Shapes the Developing Infant Gut Microbiome. Cell Host Microbe *24*, 133–145.e5.

Ganal-Vonarburg, S.C., Hornef, M.W., and Macpherson, A.J. (2020). Microbial–host molecular exchange and its functional consequences in early mammalian life. Science *368*, 604–607.

Gaspar, J.M. (2018a). NGmerge: merging paired-end reads via novel empirically-derived models of sequencing errors. BMC Bioinformatics *19*, 536.

Gaspar, J.M. (2018b). Improved peak-calling with MACS2. bioRxiv. https://doi.org/10.1101/496521.

Gensollen, T., Iyer, S.S., Kasper, D.L., and Blumberg, R.S. (2016). How colonization by microbiota in early life shapes the immune system. Science *352*, 539–544.

Gluckman, P.D., Hanson, M.A., Cooper, C., and Thornburg, K.L. (2008). Effect of in utero and early-life conditions on adult health and disease. N. Engl. J. Med. *359*, 61–73.

Gopalakrishna, K.P., Macadangdang, B.R., Rogers, M.B., Tometich, J.T., Firek, B.A., Baker, R., Ji, J., Burr, A.H.P., Ma, C., Good, M., et al. (2019). Maternal IgA protects against the development of necrotizing enterocolitis in preterm infants. Nat. Med. *25*, 1110–1115.

Harbour, S.N., DiToro, D.F., Witte, S.J., Zindl, C.L., Gao, M., Schoeb, T.R., Jones, G.W., Jones, S.A., Hatton, R.D., and Weaver, C.T. (2020). T_H17 cells require ongoing classic IL-6 receptor signaling to retain transcriptional and functional identity. Sci. Immunol. *5*, 1–17.

Harris, N.L., Spoerri, I., Schopfer, J.F., Nembrini, C., Merky, P., Massacand, J., Urban, J.F., Jr., Lamarre, A., Burki, K., Odermatt, B., et al. (2006). Mechanisms of neonatal mucosal antibody protection. J. Immunol. *177*, 6256–6262.

Hsiao, E.Y. (2014). Gastrointestinal issues in autism spectrum disorder. Harv. Rev. Psychiatry *22*, 104–111.

Hsiao, E.Y., McBride, S.W., Chow, J., Mazmanian, S.K., and Patterson, P.H. (2012). Modeling an autism risk factor in mice leads to permanent immune dysregulation. Proc. Natl. Acad. Sci. USA *109*, 12776–12781.

Hsiao, E.Y., McBride, S.W., Hsien, S., Sharon, G., Hyde, E.R., McCue, T., Codelli, J.A., Chow, J., Reisman, S.E., Petrosino, J.F., et al. (2013). Microbiota modulate behavioral and physiological abnormalities associated with neurodevelopmental disorders. Cell *155*, 1451–1463.

Ivanov, I.I., Atarashi, K., Manel, N., Brodie, E.L., Shima, T., Karaoz, U., Wei, D., Goldfarb, K.C., Santee, C.A., Lynch, S.V., et al. (2009). Induction of intestinal Th17 cells by segmented filamentous bacteria. Cell *139*, 485–498.

Kalish, B.T., Kim, E., Finander, B., Duffy, E.E., Kim, H., Gilman, C.K., Yim, Y.S., Tong, L., Kaufman, R.J., Griffith, E.C., et al. (2021). Maternal immune activation in mice disrupts proteostasis in the fetal brain. Nat. Neurosci. *24*, 204–213.

Kellermayer, R. (2012). Epigenetics and the developmental origins of inflammatory bowel diseases. Can. J. Gastroenterol. *26*, 909–915.

Kim, S., Kim, H., Yim, Y.S., Ha, S., Atarashi, K., Tan, T.G., Longman, R.S., Honda, K., Littman, D.R., Choi, G.B., and Huh, J.R. (2017). Maternal gut bacteria promote neurodevelopmental abnormalities in mouse offspring. Nature *549*, 528–532.

Klindworth, A., Pruesse, E., Schweer, T., Peplies, J., Quast, C., Horn, M., and Glöckner, F.O. (2013). Evaluation of general 16S ribosomal RNA gene PCR primers for classical and next-generation sequencing-based diversity studies. Nucleic Acids Res. *41*, e1.

Koh, A., De Vadder, F., Kovatcheva-Datchary, P., and Bäckhed, F. (2016). From dietary fiber to host physiology: Short-chain fatty acids as key bacterial metabolites. Cell *165*, 1332–1345.

Kohane, I.S., McMurry, A., Weber, G., MacFadden, D., Rappaport, L., Kunkel, L., Bickel, J., Wattanasin, N., Spence, S., Murphy, S., and Churchill, S. (2012). The co-morbidity burden of children and young adults with autism spectrum disorders. PLoS ONE *7*, e33224.

Koroleva, E.P., Halperin, S., Gubernatorova, E.O., Macho-Fernandez, E., Spencer, C.M., and Tumanov, A.V. (2015). Citrobacter rodentium-induced colitis: A robust model to study mucosal immune responses in the gut. J. Immunol. Methods *421*, 61–72.

Korpela, K., Helve, O., Kolho, K.L., Saisto, T., Skogberg, K., Dikareva, E., Stefanovic, V., Salonen, A., Andersson, S., and de Vos, W.M. (2020). Maternal Fecal Microbiota Transplantation in Cesarean-Born Infants Rapidly Restores Normal Gut Microbial Development: A Proof-of-Concept Study. Cell *183*, 324–334.e5.

Lammert, C.R., Frost, E.L., Bolte, A.C., Paysour, M.J., Shaw, M.E., Bellinger, C.E., Weigel, T.K., Zunder, E.R., and Lukens, J.R. (2018). Cutting Edge: Critical Roles for Microbiota-Mediated Regulation of the Immune System in a Prenatal Immune Activation Model of Autism. J. Immunol. *201*, 845–850.

Langmead, B., and Salzberg, S.L. (2012). Fast gapped-read alignment with Bowtie 2. Nat. Methods *9*, 357–359.

Lee, B.K., Magnusson, C., Gardner, R.M., Blomström, Å., Newschaffer, C.J., Burstyn, I., Karlsson, H., and Dalman, C. (2015). Maternal hospitalization with infection during pregnancy and risk of autism spectrum disorders. Brain Behav. Immun. *44*, 100–105.

Lee, Y., Awasthi, A., Yosef, N., Quintana, F.J., Xiao, S., Peters, A., Wu, C., Kleinewietfeld, M., Kunder, S., Hafler, D.A., et al. (2012). Induction and molecular signature of pathogenic TH17 cells. Nat. Immunol. *13*, 991–999.

Li, W., Chen, M., Feng, X., Song, M., Shao, M., Yang, Y., Zhang, L., Liu, Q., Lv, L., and Su, X. (2021). Maternal immune activation alters adult behavior, intestinal integrity, gut microbiota and the gut inflammation. Brain Behav. *11*, e02133.

Love, M.I., Huber, W., and Anders, S. (2014). Moderated estimation of fold change and dispersion for RNA-seq data with DESeq2. Genome Biol. *15*, 550.

Malkova, N.V., Yu, C.Z., Hsiao, E.Y., Moore, M.J., and Patterson, P.H. (2012). Maternal immune activation yields offspring displaying mouse versions of the three core symptoms of autism. Brain Behav. Immun. *26*, 607–616.

Maloy, K.J., Salaun, L., Cahill, R., Dougan, G., Saunders, N.J., and Powrie, F. (2003). CD4+CD25+ T(R) cells suppress innate immune pathology through cytokine-dependent mechanisms. J. Exp. Med. *197*, 111–119.

Mead, J., and Ashwood, P. (2015). Evidence supporting an altered immune response in ASD. Immunol. Lett. *163*, 49–55.

Moore, S.E., Collinson, A.C., Tamba N'Gom, P., Aspinall, R., and Prentice, A.M. (2006). Early immunological development and mortality from infectious disease in later life. Proc. Nutr. Soc. *65*, 311–318.

Osbelt, L., Thiemann, S., Smit, N., Lesker, T.R., Schröter, M., Gálvez, E.J.C., Schmidt-Hohagen, K., Pils, M.C., Mühlen, S., Dersch, P., et al. (2020). Variations in microbiota composition of laboratory mice influence Citrobacter rodentium infection via variable short-chain fatty acid production. PLoS Pathog. *16*, e1008448.

Picelli, S., Faridani, O.R., Björklund, A.K., Winberg, G., Sagasser, S., and Sandberg, R. (2014). Full-length RNA-seq from single cells using Smart-seq2. Nat. Protoc. *9*, 171–181.

Powrie, F., Leach, M.W., Mauze, S., Caddle, L.B., and Coffman, R.L. (1993). Phenotypically distinct subsets of CD4+ T cells induce or protect from chronic intestinal inflammation in C. B-17 scid mice. Int. Immunol. *5*, 1461–1471.

Prescott, S.L., Wickens, K., Westcott, L., Jung, W., Currie, H., Black, P.N., Stanley, T.V., Mitchell, E.A., Fitzharris, P., Siebers, R., et al.; Probiotic Study Group (2008). Supplementation with Lactobacillus rhamnosus or Bifidobacterium lactis probiotics in pregnancy increases cord blood interferon-γ and breast milk transforming growth factor-β and immunoglobin A detection. Clin. Exp. Allergy *38*, 1606–1614.

Ramanan, D., Sefik, E., Galván-Peña, S., Wu, M., Yang, L., Yang, Z., Kostic, A., Golovkina, T.V., Kasper, D.L., Mathis, D., and Benoist, C. (2020). An Immunologic Mode of Multigenerational Transmission Governs a Gut Treg Setpoint. Cell *181*, 1276–1290.e13.

Ramírez, F., Ryan, D.P., Grüning, B., Bhardwaj, V., Kilpert, F., Richter, A.S., Heyne, S., Dündar, F., and Manke, T. (2016). deepTools2: a next generation web server for deep-sequencing data analysis. Nucleic Acids Res. *44* (W1), W160-5.

Reed, M.D., Yim, Y.S., Wimmer, R.D., Kim, H., Ryu, C., Welch, G.M., Andina, M., King, H.O., Waisman, A., Halassa, M.M., et al. (2020). IL-17a promotes sociability in mouse models of neurodevelopmental disorders. Nature *577*, 249–253.

Rios, D., Wood, M.B., Li, J., Chassaing, B., Gewirtz, A.T., and Williams, I.R. (2016). Antigen sampling by intestinal M cells is the principal pathway initiating mucosal IgA production to commensal enteric bacteria. Mucosal Immunol. *9*, 907–916.

Robinson, M.D., McCarthy, D.J., and Smyth, G.K. (2010). edgeR: a Bioconductor package for differential expression analysis of digital gene expression data. Bioinformatics *26*, 139–140.

Sagaidak, S., Taibi, A., Wen, B., and Comelli, E.M. (2016). Development of a real-time PCR assay for quantification of Citrobacter rodentium. J. Microbiol. Methods *126*, 76–77.

Silberger, D.J., Zindl, C.L., and Weaver, C.T. (2017). Citrobacter rodentium: a model enteropathogen for understanding the interplay of innate and adaptive components of type 3 immunity. Mucosal Immunol. *10*, 1108–1117.

Smith, S.E.P., Li, J., Garbett, K., Mirnics, K., and Patterson, P.H. (2007). Maternal immune activation alters fetal brain development through interleukin-6. J. Neurosci. *27*, 10695–10702.

Subramanian, A., Tamayo, P., Mootha, V.K., Mukherjee, S., Ebert, B.L., Gillette, M.A., Paulovich, A., Pomeroy, S.L., Golub, T.R., Lander, E.S., et al. (2005). Gene set enrichment analysis: A knowledge-based approach for interpreting genome-wide expression profiles. Proc. Natl. Acad. Sci. USA *102*, 15545–15550.

Trapnell, C., Roberts, A., Goff, L., Pertea, G., Kim, D., Kelley, D.R., Pimentel, H., Salzberg, S.L., Rinn, J.L., and Pachter, L. (2012). Differential gene and transcript expression analysis of RNA-seq experiments with TopHat and Cufflinks. Nat. Protoc. *7*, 562–578.

Wadhwa, P.D., Buss, C., Entringer, S., and Swanson, J.M. (2009). Developmental origins of health and disease: brief history of the approach and current focus on epigenetic mechanisms. Semin. Reprod. Med. *27*, 358–368.

Wang, S., Ryan, C.A., Boyaval, P., Dempsey, E.M., Ross, R.P., and Stanton, C. (2020). Maternal Vertical Transmission Affecting Early-life Microbiota Development. Trends Microbiol. *28*, 28–45.

Witzel, M., Petersheim, D., Fan, Y., Bahrami, E., Racek, T., Rohlfs, M., Puchałka, J., Mertes, C., Gagneur, J., Ziegenhain, C., et al. (2017). Chromatin-remodeling factor SMARCD2 regulates transcriptional networks controlling differentiation of neutrophil granulocytes. Nat. Genet. *49*, 742–752.

Wlodarska, M., Willing, B., Keeney, K.M., Menendez, A., Bergstrom, K.S., Gill, N., Russell, S.L., Vallance, B.A., and Finlay, B.B. (2011). Antibiotic treatment alters the colonic mucus layer and predisposes the host to exacerbated Citrobacter rodentium-induced colitis. Infect. Immun. *79*, 1536–1545.

Yu, G., Wang, L.G., Han, Y., and He, Q.Y. (2012). clusterProfiler: an R package for comparing biological themes among gene clusters. OMICS *16*, 284–287.

Zegarra-Ruiz, D.F., Kim, D.V., Norwood, K., Kim, M., Wu, W.H., Saldana-Morales, F.B., Hill, A.A., Majumdar, S., Orozco, S., Bell, R., et al. (2021). Thymic development of gut-microbiota-specific T cells. Nature *594*, 413–417.

Zinkernagel, R.M. (2001). Maternal antibodies, childhood infections, and autoimmune diseases. N. Engl. J. Med. *345*, 1331–1335.

STAR★METHODS

KEY RESOURCES TABLE

REAGENT or RESOURCE	SOURCE	IDENTIFIER
Antibodies		
anti-mouse CD45 (Clone ID 30-F11) APC-Cy7	BD Biosciences	Cat# 557659; RRID: AB_396774
anti-mouse CD4 (Clone ID RM4-5) BV421	BioLegend	Cat# 100544; RRID: AB_11219790
anti-mouse CD4 (Clone ID RM4-5) BB700	BD Biosciences	Cat# 566407; RRID: AB_2744427
anti-mouse CD4 (Clone ID RM4-5) A700	Thermo Fisher Scientific	Cat# 56-0042-82; RRID: AB_494000
anti-mouse TCRβ (Clone ID H57-597) A700	BioLegend	Cat# 109224; RRID: AB_1027648
anti-mouse TCRβ (Clone ID H57-597) BV605	BioLegend	Cat# 109241; RRID: AB_2629563
anti-mouse CD8a (Clone ID 53-6.7) BV605	BioLegend	Cat# 100744; RRID: AB_2562609
anti-mouse CD8a (Clone ID 53-6.7) PerCP-Cy5.5	Thermo Fisher Scientific	Cat# 45-0081-82; RRID: AB_1107004
anti-mouse CD19 (Clone ID 6D5) BV605	BioLegend	Cat# 115540; RRID: AB_2563067
anti-mouse CD19 (Clone ID 1D3) PerCP-Cy5.5	Thermo Fisher Scientific	Cat# 45-0193-82; RRID: AB_1106999
anti-mouse IL-17A (Clone ID eBio17B7) PE-Cy7	Thermo Fisher Scientific	Cat# 25-7177-82; RRID: AB_10732356
anti-mouse IL-17A (Clone ID TC11-18H10.1) A488	BioLegend	Cat# 506910; RRID: AB_536012
anti-mouse IFN-γ (Clone ID XMG1.2) BV421	BioLegend	Cat# 505830; RRID: AB_2563105
anti-mouse RORγt (Clone ID B2D) APC	Thermo Fisher Scientific	Cat# 17-6981-82; RRID: AB_2573254
anti-mouse RORγt (Clone ID B2D) PE	Thermo Fisher Scientific	Cat# 12-6981-82; RRID: AB_10807092
anti-mouse FoxP3 (Clone ID FJK-16s) FITC	Thermo Fisher Scientific	Cat# 11-5773-82; RRID: AB_465243
anti-mouse FoxP3 (Clone ID FJK-16s) PE	Thermo Fisher Scientific	Cat# 12-5773-82; RRID: AB_465936
anti-mouse FoxP3 (Clone ID FJK-16s) APC	Thermo Fisher Scientific	Cat# 17-5773-82; RRID: AB_469457
anti-mouse CD62L (Clone ID MEL-14) FITC	Thermo Fisher Scientific	Cat# 11-0621-85; RRID: AB_465110
anti-mouse CD44 (Clone ID IM7) APC	Thermo Fisher Scientific	Cat# 17-0441-83; RRID: AB_469391
anti-mouse CD25 (Clone ID PC61.5) PE-Cy7	Thermo Fisher Scientific	Cat# 25-0251-82; RRID: AB_469608
anti-mouse CD45RB (Clone ID 16A) PE	BD Biosciences	Cat# 553101; RRID: AB_394627
IL-17A-blocking antibody (Clone ID 50104)	R&D systems	Cat# MAB421; RRID: AB_2125018
Isotype control antibody (Clone ID 54447)	R&D systems	Cat# MAB006; RRID: AB_357349
Purified anti-mouse CD3e (Clone ID 145-2V11)	Tonbo Biosciences	Cat# 70-0031; RRID: AB_2621472
Bacterial and virus strains		
Citrobacter rodentium (Strain: DBS100)	ATCC	Cat# 51459
Chemicals, peptides, and recombinant proteins		
Poly(I:C) potassium salt	Sigma Aldrich	Cat# P9582
Poly(I:C) sodium salt	Sigma Aldrich	Cat# P1530
Liberase-TM research grade	Millipore Sigma	Cat# 5401127011
DNase I	Millipore Sigma	Cat# 10104159001
PMA	Sigma Aldrich	Cat# P1585
Ionomycin	Sigma Aldrich	Cat# I0634
Golgiplug	BD Biosciences	Cat# 555029
Metronidazole	Sigma Aldrich	Cat# 1442009
MacConkey Agar	Fisher Scientific	Cat# B11387
DSS	TdB labs	Cat# 9011-18-1
DTT	Millipore Sigma	Cat# 10708984001
EDTA 0.5M pH 8.0	Corning	Cat# 46-034-CI
FBS	Hyclone	Cat# SH30910.03
FBS	Corning	Cat# 35-010-CV
Percoll	Sigma Aldrich	Cat# GE17-0891-01

(*Continued on next page*)

Continued

REAGENT or RESOURCE	SOURCE	IDENTIFIER
Bouin's fixative	Electron Microscopy Science	Cat# 15990-01
TCL buffer	QIAGEN	Cat# 1031576
Critical commercial assays		
Mouse IL-17A enhanced sensitivity flex set	BD Biosciences	Cat# 562261
Mouse IFN-γ enhanced sensitivity flex set	BD Biosciences	Cat# 562233
Mouse TNF enhanced sensitivity flex set	BD Biosciences	Cat# 562336
Mouse IL-6 enhanced sensitivity flex set	BD Biosciences	Cat# 562236
Hooke Kit MOG_{35-55}/CFA Emulsion PTX	Hooke Laboratories	Cat# EK-2110
RNeasy micro kit	QIAGEN	Cat# 74004
iScript reverse transcription kit	Bio-Rad	Cat# 1708891
iTaq SYBR green mix	Bio-Rad	Cat# 1725125
Nextera XT DNA Library preparation kit	Illumina	Cat# FC-131-1096
Illumina Tagment DNA Enzyme and Buffer Kit	Illumina	Cat# 15027865, Cat# 15027866
MinElute PCR Purification Kit	QIAGEN	Cat# 28004
PCR purification kit, AMPure XP	Beckman Coulter	Cat# A63880
eBioscience Foxp3/ Transcription Factor Staining Buffer Kit	Thermo Fisher Scientific	Cat# 00-5523-00
LIVE/DEAD Fixable Aqua Dead Cell stain kit	Thermo Fisher Scientific	Cat# L34966
Deposited data		
16S rRNA sequencing	This paper	Accession# PRJNA694443
ATAC-seq	This paper	Accession# GSE165692
RNA-seq	This paper	Accession# GSE165693
Experimental models: Organisms/strains		
C57BL/6 specific pathogen-free mice	Taconic	Cat# B6 (C57BL/6NTac)
C57BL/6 Germ-free mice	Charles River (maintained in GF isolators at Harvard Medical School)	Cat# C57BL/6NCrl
RAG1-deficient mice	Jackson Laboratory	Cat# 002216
CD45.1 B6.SJL congenic mice	Taconic	Cat# 4007 (B6.SJL-*Ptprc*^{a}/BoyAiTac)
IL-17A-GFP reporter mice	Jackson Laboratory	Cat# 018472
Oligonucleotides		
16S rRNA sequencing V3 and V4 amplicon primers Forward: 5′-TCGTCGGCAGCGTCA GATGTGTATAAGAGACAGCCTACGGGNG GCWGCAG-3′, Reverse: 5′- GTCTCGTGGG CTCGGAGATGTGTATAAGAGACAGGACTA CHVGGGTATCTAATCC-3′	Klindworth et al., 2013	N/A
16S Universal primers Forward: 5′-ACTCCT ACGGGAGGCAGCAGT-3′, Reverse: 5′- ATT ACCGCGGCTGCTGGC-3′	This paper	N/A
espB primers Forward: 5′-ATGCCGCAGAT GAGACAGTTG-3′, Reverse: 5′- CGTCAGC AGCTTTTCAGCTA-3′	Sagaidak et al., 2016	N/A
Mouse Gapdh qPCR primers Forward: 5′- CATCACTGCCACCCAGAAGACTG-3′, Reverse: 5′- ATGCCAGTGAGCTTCCCGTTCAG-3′	Origene	Cat# MP205604
Mouse Brd4 qPCR primers Forward: 5′- GCCATCTACACTACGAGAGTTGG-3′, Reverse: 5′- ATTCGCTGGTGCTCTCCGACTC-3′	Origene	Cat# MP201449
Mouse Il6ra qPCR primers Forward: 5′- TGCAGTTCCAGCTTCGATACCG-3′, Reverse: 5′- TGCTTCACTCCTCGCAAGGCAT-3′	Origene	Cat# MP206799

(*Continued on next page*)

Continued

REAGENT or RESOURCE	SOURCE	IDENTIFIER
Mouse Map4k2 qPCR primers Forward: 5′- GGCTACTCTGAAGCAACAGGAG-3′, Reverse: 5′- GCAGCCATTGAAGACCTTGGAG-3′	Origene	Cat# MP208352
Mouse Smarcd2 qPCR primers Forward: 5′- CTTTCGAGAGGAAGCTGGACCA-3′, Reverse: 5′- GTTCCCGCATTATCTCCATCCG-3′	Origene	Cat# MP220661
Mouse Zbtb7a qPCR primers Forward: 5′- TGCGAGAAGGTGATTCAGGGTG-3′, Reverse: 5′- TTCCGCATGTGCACCTTCAGCT-3′	Origene	Cat# MP218697
Software and algorithms		
EthoVision XT 14	Noldus	https://www.noldus.com
Multiplot studio v1.5.20	Genepattern Archive	http://gparc.org
R v4.0.5	R foundation for statistical computing	https://cran.r-project.org
FlowJo 10	BD	https://www.flowjo.com
Prism 9	GraphPad	https://www.graphpad.com
QIIME2 v2020.02	Bolyen et al., 2019	https://qiime2.org
Dada2	Callahan et al., 2016	https://benjjneb.github.io/dada2
NGmerge	Gaspar, 2018a	https://github.com/jsh58/NGmerge
Bowtie2 v2.3.4.3	Langmead and Salzberg, 2012	http://bowtie-bio.sourceforge.net/bowtie2/
Picard v2.8.0	N/A	https://broadinstitute.github.io/picard/
removeChrom.py	N/A	https://github.com/harvardinformatics/ATAC-seq/blob/master/atacseq/removeChrom.py
Samtools v1.9	N/A	http://www.htslib.org
MACS peak caller v2.1.1.20160309	Gaspar, 2018b	https://pypi.org/project/MACS2/2.1.1.20160309/
ChIPseeker v1.24.0	N/A	https://bioconductor.org/packages/release/bioc/html/ChIPseeker.html
Deeptools2	Ramírez et al., 2016	https://github.com/deeptools/deepTools
clusterProfiler v3.16.0	Yu et al., 2012	https://guangchuangyu.github.io/software/clusterProfiler/

RESOURCE AVAILABILITY

Lead contact

Further information and requests for resources and reagents should be directed to and will be fulfilled by the lead contact, Jun R. Huh (jun_huh@hms.harvard.edu).

Materials availability

This study did not generate new unique reagents.

Data and code availability

- The RNA-seq, ATAC-seq and 16S rRNA sequencing data have been deposited at NCBI Sequence Read Archive and Gene Expression Omnibus and are publicly available as of the date of publication. Accession numbers are listed in the key resource table.
- This paper does not report original code.
- Any additional information required to reanalyze the data reported in this paper is available from the lead contact upon request.

EXPERIMENTAL MODEL AND SUBJECT DETAILS

Mice

All animals were housed in an individually ventilated cage system (Tecniplast), a specific pathogen-free facility maintained at 20–22°C and 40%–55% humidity and under a 12-h light/12-h dark cycle. All experiments were conducted in accordance with procedures approved by the Institutional Animal Care and Use Committee of Harvard University. All wild-type (WT) conventional C57BL/6 mice were purchased from Taconic Biosciences IBU21 (USA). GF C57BL/6 mice were purchased from Charles River Laboratories and maintained in GF isolators at Harvard Medical School. For immunological analyses, including EAE and colitis experiments, 4–9-week-old male and female mice were used. For time-mating and behavioral tests, 8–20-weeks old male and female mice were used.

METHOD DETAILS

Maternal immune activation

C57BL/6 male mice were mated overnight with 8–12-week-old C57BL/6 females carrying a mouse commensal SFB (Kim et al., 2017). At E12.5, pregnant mice were weighed and injected with a single dose (20 mg per kg, intraperitoneal injection) of poly(I:C) (P9582 or P1530, Sigma Aldrich) or phosphate-buffered saline (PBS). Each dam was returned to its home cage and left undisturbed until the birth of her litter. All pups remained with the mother until weaning on postnatal days 21–28, at which time mice were group-housed at a maximum of five per cage with the same-sex littermates. SFB-mono-PBS and SFB-mono-MIA offspring were born inside the flexible film isolators and raised by SFB-mono-colonized pregnant dams injected with PBS or poly(I:C). For the behavioral assays and *C. rodentium* infection experiments, the mice were moved to the Tecniplast isocage system. For the IL-17 cytokine blockade experiment, a monoclonal IL-17A-blocking antibody (clone 50104, R&D) or an isotype control antibody (IgG2a, clone 54447, R&D) was intraperitoneally injected (500 μg per animal) 5 h prior to PBS or poly(I:C) administration (Choi et al., 2016).

Citrobacter rodentium infection

Seven to nine-week-old mice were orally gavaged with 200 μL of 1 mg/ml metronidazole for 4 days before infection with *C. rodentium* (Wlodarska et al., 2011). On the day of infection, 2×10^8 CFUs of *C. rodentium* (DBS 100) resuspended in 100 μL PBS were orally administered to mice. Germ-free mice were infected with 1×10^6 CFUs of *C. rodentium.* Bacterial CFUs were counted by dilution plating on MacConkey agar (Koroleva et al., 2015). Additionally, qPCR was used for measuring *espB*, a *C. rodentium*-encoded gene (Sagaidak et al., 2016). Bacterial genomic DNA was isolated from the fecal pellets of mice with phenol-chloroform extraction. Undetected qPCR values from non-colonized samples were replaced with a Ct value of 40 for comparison, and *espB* Cq values were normalized with universal 16S Cq values. Primer sequences are provided in the Key resources table.

Cytometric bead array

Plasma concentrations of IL-6, IFN-γ, TNF, and IL-17A were measured by enhanced sensitivity cytometric bead array kit according to the manufacturer's protocol (BD Biosciences).

Isolation of lamina propria lymphocytes

Colon tissues were collected and incubated with 1 mM dithiothreitol (DTT), 1 mM ethylenediaminetetraacetic acid (EDTA), and 2% fetal bovine serum (FBS) in Hank's Balanced Salt Solution (HBSS), at 37°C for 15 min with constant shaking to remove mucus and epithelial cells. The remaining tissues were dissociated in digestion buffer (RPMI 1640 media, 62.5 μg/ml Liberase [Roche], 50 μg/ml DNase I [Sigma Aldrich], and 2% FBS) with constant stirring at 37°C for 45 min. Mononuclear cells were collected at the interface of a 40%/80% Percoll gradient (GE Healthcare). Cells were then analyzed by flow cytometry.

Flow cytometry

Antibodies that were used for flow cytometry are listed in the Key resources table. Isolated immune cells from the mesenteric lymph nodes and the intestines of mice were stimulated with 50 ng/ml of phorbol 12-myristate 13-acetate (PMA) (Sigma Aldrich) and 1 μM ionomycin (Sigma Aldrich) in the presence of GolgiPlug (BD Biosciences) for 3 h to determine cytokine expression. After stimulation, cells were stained with antibodies against cell-surface markers and the LIVE/DEAD fixable dye Aqua (Thermo Fisher Scientific) to exclude dead cells, fixed and permeabilized with a FoxP3 transcription factor staining kit (eBioscience), and subsequently stained with cytokine- and/or transcription factor-specific antibodies. All flow cytometry analyses were performed on an LSR II or Symphony flow cytometer (BD), and data were analyzed with FlowJo software (BD).

Tissue histology

For assessing colon histopathology, dissected colon tissues were fixed in Bouin's fixative (Electron Microscopy Science). Hematoxylin and eosin (H & E) staining and disease scoring were performed by the Rodent Histopathology Core at Harvard Medical School. In brief, representative longitudinal sections of the distal colon were stained with hematoxylin and eosin and graded using a scheme based on that described by Maloy et al. (2003). Each sample was scored semiquantitatively according to a grade scale of 0–3. Typical grade features are: 0 = normal; 1 = mild epithelial hyperplasia and inflammatory infiltrates; 2 = pronounced hyperplasia and significant inflammatory infiltrates; 3 = severe hyperplasia and infiltration with a significant decrease in goblet cells.

Dextran sodium sulfate-induced colitis

Mice were administered 2.5% DSS (approximately 40 kDa; TdB Labs) in their drinking water for seven days and then changed to regular water. Weight loss was monitored daily. Colon length and histology were analyzed at day fourteen post-treatment.

Experimental autoimmune encephalomyelitis model

Twelve-week-old PBS and MIA female offspring were subjected to EAE induction using MOG35-55 and complete Freund's adjuvant (CFA) emersion pertussis toxin (PTX) kit (Hooke Laboratories). 80 ng of PTX was used for this particular experiment. EAE clinical symptoms were scored according to the manufacturer's scoring guidelines.

Anti-CD3 induced inflammation

IL-17A-GFP heterozygote PBS and MIA offspring were generated by crossing IL-17A-GFP homozygous males with C57BL/6 females carrying SFB. Five-to-six-week-old offspring born from this mating were injected with anti-CD3 (20 μg per mouse). Body weight change was monitored every day. Three days later, mice were euthanized, and ~6 cm of proximal small intestines were harvested for lamina propria immune cell analysis (Esplugues et al., 2011).

Three-chamber social approach assay

Seven to eight-week-old male mice were tested for social behavior using a three-chamber assay. A day before the test, experimental mice were introduced into a three-chamber arena (50 cm x 35 cm x 30 cm) with two empty containment cages (circular metallic cages, Stoelting Neuroscience) for a 10 min acclimation phase. The following day, the mice underwent a 5 min exploration period with empty containment cages. Immediately after, the mice were confined to the center chamber, while a social object (unfamiliar C57BL/6 male mouse) and an inanimate object (a similar-sized rubber object to the social object) were placed in each containment cage. Barriers to the adjacent chambers were removed, and the experimental mice were given 10 min to explore both chambers and measured for approach behavior as interaction time (i.e., sniffing, approach) with targets in each chamber (within 2 cm). Sessions were video-recorded, and object exploration time and total distance moved were analyzed using the Noldus tracking system. Arenas and contents were thoroughly cleaned between testing sessions. Multiple social targets from different home cages were used for testing to prevent potential odorant confounds from target home cages.

Marble-burying test

Seven to eight-week-old male mice were placed in a testing arena (arena size: 40 × 20 cm^2, bedding depth: 3 cm) containing 20 glass marbles, which were laid out in five rows of four marbles equidistant from one another. At the end of a 15 min exploration period, mice were gently removed from the testing cages, and the number of marbles buried under the bedding was recorded. A marble-burying index was scored as 1 for marbles covered > 50% by bedding, 0.5 for around 50% covered, or 0 for anything less. The percentage of buried marbles is plotted on the y axis.

Cross-fostering experiments

Cross-fostering was performed within 24 h after birth. The entire litter was removed from its birth mother and transferred into a cage in which a foster dam was housed. Pups were raised by foster mothers until weaning on postnatal days 21–28.

Germ-free mouse colonization

For colonization of GF female mice with the fecal slurries from PBS or MIA pregnant dams, 100 mg of fecal samples were homogenized in 1 mL PBS using a 100 μm cell strainer and a 3 mL syringe plunger. 200 μL of supernatant (approximately equal to 20 mg of fecal pellets) was introduced into individual GF mice using a 20 G gavage needle (Cadence Science). One week after the colonization, the colonized females were mated with GF males in isocages.

Isolation of fecal bacterial microbiota and 16S rRNA gene sequencing analysis

Metagenomic 16S rRNA sequencing was performed by Omega Bioservices (Norcross, GA, USA). DNA of the mouse fecal pellets was isolated using the Omega Mag-Bind Universal Pathogen kit. DNA concentration was measured by the QuantiFluor dsDNA System on a Quantus Fluorometer (Promega). The samples were then normalized to 12.5 ng of input in 2.5 μL (5 ng/μl) and amplified using primers specific to the V3 and V4 regions: forward 5′-TCGTCGGCAGCGTCAGATGTGTATAAGAGACAGCC TACGGGNGGCWGCAG-3′, reverse 5′- GTCTCGTGGGCTCGGAGATGTGTATAAGAGACAGGACTACHVGGGTATCTAATCC-3′. The amplification was done using the KAPA HiFi HotStart ReadyMix (Kapa Biosystems). Residual primers were cleaned up using Mag-Bind RxnPure Plus magnetic beads (Omega Bio-tek). Purified amplicons were then ligated with indexing adaptors and underwent a second index PCR amplification. The libraries for each experimental group were normalized with Mag-Bind Equipure Library Normalization Kit (Omega Bio-tek) and pooled. The pooled library of ~600 bases in size was checked using an Agilent 2200 TapeStation and sequenced (2 × 300 bp paired-end read setting) on the MiSeq instrument (Illumina). FASTQ files were used in subsequent analyses. Raw FASTQ sequences were then quality filtered and analyzed by QIIME2 version 2020.02 (Bolyen et al., 2019) and Dada2 (Callahan et al., 2016). Operational taxonomic units were defined based on a sequence similarity threshold of 97%. The phylogenetic affiliation of each operational taxonomic unit was aligned to the Greengenes reference database version 13_8 and 99% ID.

Adoptive transfer of $CD45RB^{high}$ $CD4^+$ T cells

$CD45RB^{high}$ $CD4^+$ T cell adoptive transfer was performed as previously described (Powrie et al., 1993). In brief, the spleens and the lymph nodes (lateral axillary and inguinal) were dissected from 4-week-old offspring. $CD4^+$ T cells were enriched with magnetic microbeads (Miltenyi) according to the manufacturer's protocol, stained with CD4, CD25, CD45RB, CD44, and CD62L antibodies (Key resources table) and sorted for naive T cells ($CD4^+$, $TCR\beta^+$, $CD45RB^{high}$, $CD44^{low}$, $CD62L^{high}$, $CD25^{low}$) by fluorescence-activated cell sorting (FACS). 5×10^5 sorted cells were adoptively transferred into individual RAG1-deficient recipient mice by intraperitoneal (i.p.) injection.

RNA extraction and quantitative real-time PCR

Naive T cells (50,000 cells) were sorted ($CD4^+$, $TCR\beta^+$, $CD45RB^{high}$, $CD44^{low}$, $CD62L^{high}$, $CD25^{low}$), and RNA was extracted by RNeasy micro kit (QIAGEN) following the manufacturer's instructions. RNA concentration was quantified and normalized prior to cDNA synthesis. cDNA was synthesized by reverse transcription (iScript, Bio-Rad), followed by qRT-PCR (LightCycler 96, Roche Life Science) using SYBR green (iTaq universal SYBR, Bio-Rad). Primer sequences are provided in the Key resources table.

RNA-seq experiments

RNA-seq was performed with the standard ImmGen low-input protocol. A total of 1,000 cells were sorted directly into 5 μl of lysis buffer (TCL Buffer [QIAGEN] with 1% 2-Mercaptoethanol). Smart-seq2 libraries were prepared as previously described (Picelli et al., 2014) with slight modifications. Briefly, total RNA was captured and purified on RNAClean XP beads (Beckman Coulter). Polyadenylated mRNA was then selected using an anchored oligo(dT) primer and converted to cDNA via reverse transcription. The first-strand cDNA was subjected to limited PCR amplification followed by Tn5 transposon-based fragmentation using the Nextera XT DNA Library Preparation Kit (Illumina). Samples were then PCR amplified for 18 cycles using barcoded primers such that each sample carries a specific combination of eight base Illumina P5 and P7 barcodes for subsequent pooling and sequencing. Paired-end sequencing was performed on an Illumina NextSeq 500 using 2 × 25 bp reads. Reads were aligned to the mouse genome, Gencode GRCm38 primary assembly. Transcripts were quantified by the Broad Technology labs computational pipeline with Cuffquant version 2.2.1 (Trapnell et al., 2012). Raw sequencing read counts were normalized by the median of ratios method with the DESeq2 package (Love et al., 2014) from Bioconductor then converted to GCT and CLS format (https://www.genepattern.org/file-formats-guide). Normalized reads were further filtered by minimal expression and analyzed by Multiplot Studio in the GenePattern software package (https://www.genepattern.org/modules/docs/Multiplot/2). Gene ontology analysis and gene set enrichment analysis (Subramanian et al., 2005) were performed by clusterProfiler (v.3.16.0) (Yu et al., 2012).

ATAC-seq experiments

Standard ATAC-seq was performed according to a published protocol (Buenrostro et al., 2013). In brief, we sorted 50,000 naive $CD4^+$ T cells in a 1.5 mL LoBind microcentrifuge tube (Eppendorf), centrifuged the sorted cells at 500 × g for 5 min at 4°C, and then removed the supernatant without disrupting the cell pellet. The cells were washed once with 50 μL of cold PBS buffer and centrifuged at 500 × g for 5 min at 4°C, followed by supernatant removal. Cells were lysed using 50 μl chilled lysis buffer (10 mM Tris-HCl, pH 7.5, 10 mM NaCl, 3 mM $MgCl_2$, 0.1% NP-40, 0.1% Tween-20, and 0.01% digitonin). After incubating 3 min on ice, 1 mL wash buffer (10 mM Tris-HCl, pH 7.5, 10 mM NaCl, 3 mM MgCl2, and 0.1% Tween-20) was added and centrifuged 5 min at 500 × g, 4°C. After discarding the supernatant, the pellet was resuspended in the transposase reaction mix (25 μL 2 × TD buffer, 2.5 μL transposase [Illumina], 16.5 μL PBS, 0.1% Tween-20, 0.01% digitonin, and 5 μL nuclease-free water). The transposition reaction was carried out for 30 min at 37°C. Directly following transposition, the sample was purified using a QIAGEN MinElute kit. Following purification, we amplified library fragments using 1 × NEBnext PCR master mix and 1.25 μM of custom Nextera PCR primers under the following PCR conditions: 72°C for 5 min; 98°C for 30 s; and thermocycling at 98°C for 10 s, 63°C for 30 s, and 72°C for 1 min. The amplification cycle was determined based on the amplification curve on qPCR. Primer dimers were removed by AMPure XP beads selection (Beckman Coulter). After determining the quality on an Agilent High-Sensitivity DNA Bioanalysis chip, the library was loaded onto an Illumina NextSeq 500 sequencer for 75 bp paired-end sequencing, aiming for 5×10^6 reads per sample.

The basecall files were demultiplexed through the BioPolymer Facility's pipeline, and the resulting FASTQ files were used in subsequent analyses. Raw FASTQ files were processed following ATAC-seq Guidelines published from the Harvard Faculty of Arts and Sciences Informatics Core. In brief, after the removal of adaptors by NGmerge (Gaspar, 2018a), sequencing reads were aligned to the *Mus musculus* 10 (mm10, downloaded from ENSEMBL) using Bowtie2 (v2.3.4.3) (Langmead and Salzberg, 2012). PCR duplicates were removed using Picard (v2.8.0). Reads mapped to mitochondrial DNA were excluded by removeChrom.py, and non-uniquely mapped reads were also removed using a mapping quality score < 10 on samtools (v1.9). Peaks were identified using the MACS peak caller (v2.1.1.20160309) (Gaspar, 2018b). Differential accessibility was performed with ATAC-seq counts from PBS and MIA biological replicates using a quasi-likelihood F-test employed by the glmQLFit and glmQLFTest functions (Robinson et al., 2010). ATAC-seq open chromatin regions with a minimum fold change of 1.5 and FDR < 0.05 were considered significant. ChIPseeker (v1.24.0) was used to annotate the peaks. ATAC-seq heatmaps and aggregated plots were generated using deeptools2 (Ramírez et al., 2016). Gene ontology analysis was performed by clusterProfiler (v.3.16.0) (Yu et al., 2012).

QUANTIFICATION AND STATISTICAL ANALYSIS

Statistical analyses were performed with Prism v.9.0.0 (GraphPad). For two-group comparisons, the statistical significance was determined by unpaired Student's t test. For three or more group comparisons, the statistical significance was determined by one-way ANOVA. For multi-factor comparison, the statistical significance was determined by two-way ANOVA. All the statistical parameters of experiments can be found in each figure legend and Table S1. Each data point denotes individual animals. Error bars represent ± standard error of the mean (SEM).